Contributions to Mineralogy and Petrology (2020) 175:74
https://doi.org/10.1007/s00410-020-01712-1

ORIGINAL PAPER

Resubduction of lawsonite eclogite within a serpentinite-filled subduction channel

R. Tamblyn[1] · M. Hand[1] · L. Morrissey[2] · T. Zack[1,3] · G. Phillips[4] · D. Och[5]

Received: 31 January 2020 / Accepted: 2 July 2020 / Published online: 17 July 2020

Abstract

Translating burial and exhumation histories from the petrological and geochronological record of high-pressure assemblages in subduction channels is key to understanding subduction channel processes. Convective return flow, either serpentinite or sediment hosted, has been suggested as a potential mechanism to retrieve rocks from significant depths and exhume them. Numerical modelling predicts that during convective flow, subducted material can be cycled within a serpentinite-filled subduction channel. Geochronological and petrological evidences for such cycling during subduction are preserved in lawsonite eclogite from serpentinite melange in the Southern New England Orogen, eastern Australia. Ar–Ar, Rb–Sr phengite and U–Pb titanite geochronology, supported by phase equilibrium forward modelling and mineral zoning, suggest Cambro–Ordovician eclogite underwent two stages of burial separated by a stage of partial exhumation. The initial subduction of the eclogite at ca. 490 Ma formed porphyroblastic prograde-zoned garnet and lawsonite at approximate *P–T* conditions of at least 2.9 GPa and 600 °C. Partial exhumation to at least 2.0 GPa and 500 °C is recorded by garnet dissolution. Reburial of the eclogite resulted in growth of new Mg-rich garnet rims, growth of new prograde-zoned phengite and recrystallization of titanite at *P–T* conditions of approximately 2.7 GPa and 590 °C. U–Pb titanite, and Ar–Ar and Rb–Sr phengite ages constrain the timing of reburial to ca. 450 Ma. This was followed by a second exhumation event at approximately 1.9 GPa and 520 °C. These conditions fall along a cold approximate geotherm of 230 °C/GPa. The inferred changes in pressure suggest the lawsonite eclogite underwent depth cycling within the subduction channel. Geochronological data indicate that partial exhumation and reburial occurred over ca. 50 M y., providing some estimation on the timescales of material convective cycling in the subduction channel.

Keywords Eclogite · Lawsonite · Resubduction · High pressure · Corner flow · Port Macquarie

Introduction

Metamorphism along cool geothermal gradients in subduction zones produces eclogite-facies mineral assemblages. These assemblages often preserve an abundance of prograde, peak and retrograde petrological relationships. For example, elemental zoning in garnet and micas can be preserved due to slow rates of diffusion, and temperature-sensitive minerals such as lawsonite can also be preserved (Tsujimori et al. 2006; Tsujimori and Ernst 2014). Given this potential to preserve extensive petrological relationship histories, methods such as phase equilibrium modelling coupled with new and emerging geochronological techniques open avenues to explore the pressure–temperature–time (*P–T–t*) histories of these high-pressure low-temperature assemblages, and make inferences about the behaviour of the subduction systems that host them.

Communicated by Steven Reddy.

Electronic supplementary material The online version of this article (https://doi.org/10.1007/s00410-020-01712-1) contains supplementary material, which is available to authorized users.

✉ R. Tamblyn
renee.tamblyn@adelaide.edu.au

[1] Department of Earth Sciences, The University of Adelaide, Adelaide, Australia

[2] School of Natural and Built Environments, The University of South Australia, Adelaide, Australia

[3] Department of Earth Sciences, University of Gothenburg, Gothenburg, Sweden

[4] Geological Survey of New South Wales, Sydney, Australia

[5] WSP Parsons Brinckerhoff, Sydney, Australia

The application of sophisticated petrological techniques to eclogite and blueschist assemblages has highlighted the potential for complex *P–T–t* histories. This is particularly apparent in serpentinite melanges. Mixing, accumulation, long-lived residence and intrachannel circulation of high-pressure lithologies have started to emerge as common phenomena within subduction channels (e.g. Krebs et al. 2008; Lázaro et al. 2009). Numerical modelling has sought to explain the dynamics of material within subduction channels, and has demonstrated that complex *P–T–t* histories are possible, arising from cycling and corner flow within the channel (Gerya et al. 2002; Stöckhert and Gerya 2005; Roda et al. 2019). Examples of high-pressure rocks that have seen two or more cycles of burial have been recognised through geochronological and mineralogical evidence, for example, dating zones within metamorphic zircon (e.g. Liati et al. 2016). However, in lieu of such useful petrochronological methods, recognising multiple burial cycles can prove difficult.

Lawsonite eclogite is globally rare, despite the range of bulk compositions that support the formation of lawsonite–garnet–omphacite (Wei and Clarke 2011). Therefore, their occurrence probably reflects unusually good preservation of deeply buried, cold subducted material. Consequently, lawsonite eclogites potentially preserve comprehensive records of the physical conditions of subduction channels. This study presents detailed petrological results from eclogite in the Southern New England Orogen (SNEO) that supports partial exhumation and reburial of a single block of lawsonite eclogite during ongoing subduction. Phase diagrams constrain the approximate pressure–temperature (*P–T*) conditions of partial exhumation and reburial within the subduction channel, which is supported by U–Pb titanite, and Rb–Sr and Ar–Ar phengite geochronological data. The cycle of exhumation and reburial records an approximate total pressure and temperature fluctuation of at least 1.6 GPa and 190 °C and is constrained to have occurred over ca. 50 M y. If the pressure fluctuations recorded by high-pressure mineral assemblages reflect oscillations in burial depths, such records support the notion of convective flow within the subduction channel.

Geological setting

The Southern New England Orogen

The Southern New England Orogen (SNEO) in eastern Australia is the youngest and most outboard orogen of the Tasmanides (Fig. 1a; Kemp et al. 2009; Glen 2013; Phillips et al. 2015). The Tasmanides are interpreted to have formed as a result of long-lived subduction on the East Gondwanan margin during the Cambrian–Triassic, which resulted in a series of eastward-younging orogens. The oldest and most westerly of these is the Delamerian Orogen, which formed at ca. 515–490 Ma on the margin of cratonic Australia, and was post-dated by the Lachlan–Thompson Orogen at ca. 484–340 Ma (Fig. 1a). The SNEO formed between the upper Devonian–Triassic, and consists of a volcanic arc, forearc basin and accretionary complex (Fig. 1b; Jenkins et al. 2002; Jessop et al. 2019). The Devonian–Carboniferous volcanic arc outcrops, but is generally obscured under the younger Permian–Triassic Sydney–Gunnedah basin (Jenkins et al. 2002). The Tamworth Belt contains a forearc basin, consisting of felsic volcanic rocks and volcaniclastics (Roberts and James 2010). The Tablelands Complex consists of deformed sediments and oceanic basalt that accumulated within an accretionary complex. These are separated by the serpentinite-bearing Peel-Manning Fault System (Fig. 1b). The SNEO also contains numerous felsic magmatic rocks of the Permian–Triassic New England Batholith, which intrude the Tablelands Complex and the Early Permian basins (Leitch 1975; Shaw and Flood 1981; Phillips et al. 2011). These are interpreted to have formed as the orogen evolved from an accretionary system to a back-arc position (Jenkins et al. 2002; Phillips et al. 2011).

Tectonic framework of the high-pressure rocks and the Tasmanides

There has been significant debate surrounding the evolution of the Tasmanides, including the tectonic significance of the high-pressure rocks. Notably, all the geochronology reported from serpentinite-hosted high-pressure exotic blocks in the SNEO is significantly older than the enclosing geology (Fig. 1b; e.g. Fukui et al. 1995, Sano et al. 2004; Phillips et al. 2015; Manton et al. 2017; Tamblyn et al. 2019a). The most coherent views about the evolution of the Tasmanides involve eastward retreat of a subduction system that formed close to the cratonic margin during the mid-late Cambrian (e.g. Collins 2002; Phillips and Offler 2011; Moresi et al. 2014; Phillips et al. 2015). The general consensus is the high-pressure rocks found in the SNEO were formed in a subduction channel on the cratonic margin of Australia during the Delamerian Orogen in the Cambrian–Ordovician. Subsequent cooling and transport of the high-pressure rocks occurred during eastward-directed slab rollback, until the high-pressure rocks were exhumed in their current location in the Permian–Triassic SNEO (Phillips and Offler 2011; Phillips et al. 2015; Tamblyn et al. 2019a). During this rollback, the Lachlan/Thompson Orogens developed in a back-arc setting on the upper plate (e.g. Collins 2002; Kemp et al. 2009; Moresi et al. 2014). Eastward younging arcs track the rollback of the subduction zone, accompanied by voluminous I and S-type magmatism formed from arc and back-arc rifting processes (Collins 2002; Collins and Richards 2008).

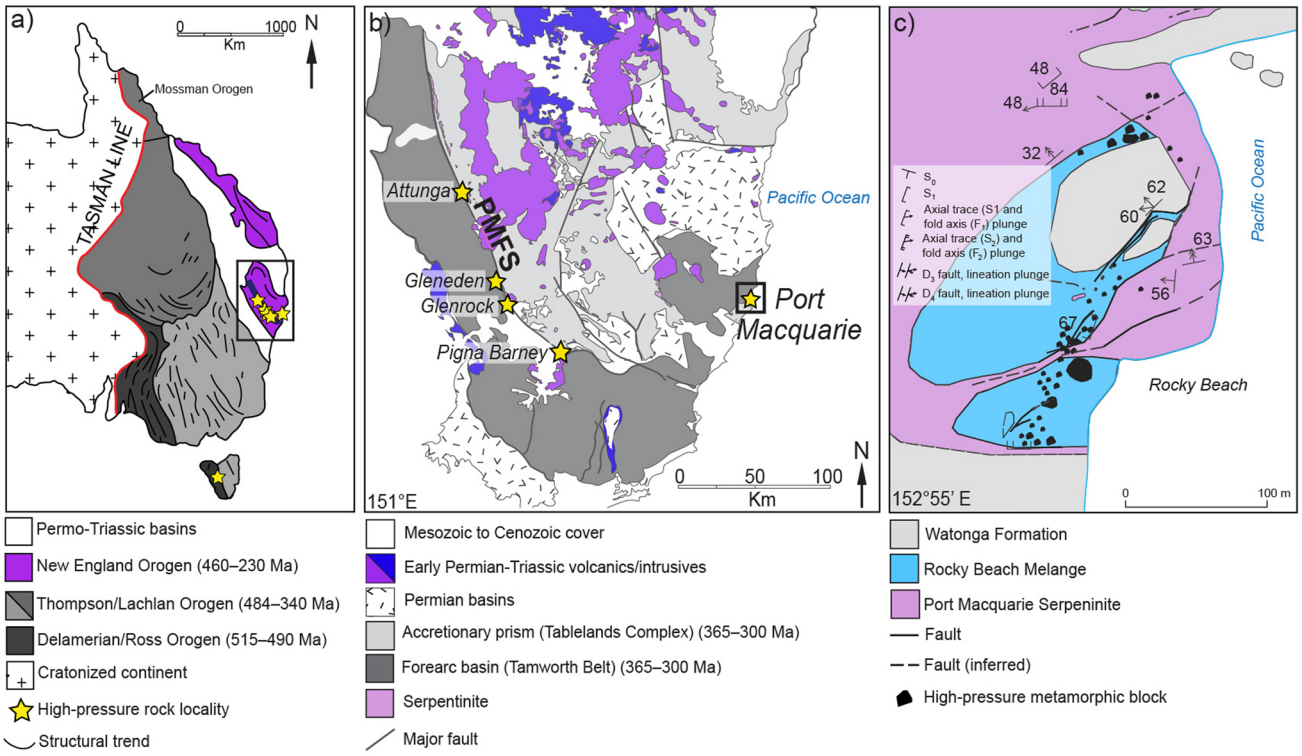

Fig. 1 **a** Simplified map of eastern Australia (east of the Tasman line) showing the main eastward-younging orogens. The SNEO is indicated in the black box. **b** Geological map of the SNEO, showing other high-pressure rock localities and indicating the location of Port Macquarie in the black box. *PMFS* peel-manning fault system. **c** Geological map of Rocky Beach at Port Macquarie, showing the high-pressure melange encased in serpentinite, modified from Och et al. (2003)

This eastward migration is also revealed in ε_{Nd} isotopes of magmatic rocks, which demonstrate an increasingly juvenile signature as the subduction zone migrated away from the cratonic margin (Kemp et al. 2009).

High-pressure metamorphism and melange formation in the SNEO

High-pressure metamorphic rocks hosted in serpentinite occur throughout the SNEO at Attunga, Gleneden, Glenrock, Pigna Barney and Port Macquarie (Fig. 1b; Phillips et al. 2015). The Port Macquarie melange contains by far the largest lithological variety of high-pressure rocks, which are described in detail by Och et al. (2003, 2007) and Tamblyn et al. (2019a). The melange consists of exotic high-pressure blocks encased in chlorite–actinolite schist, which is in turn encased within serpentinite (Fig. 1c). These exotic blocks consist of variably metamorphosed omphacitite, low-grade basaltic rocks, sedimentary rocks, marble, blueschist facies rocks, retrogressed eclogite and lawsonite-bearing eclogite. In situ U–Pb geochronology on microzircon from the lawsonite eclogite returned a range of ages from ca. 560–440 Ma (Tamblyn et al. 2019a). The zircons occur as inclusions in garnet and also occur in the surrounding matrix. Lu–Hf geochronology on lawsonite porphyroblasts gives an age of 506 ± 15 Ma, and a Lu–Hf garnet whole-rock isochron gives an age of 489.7 ± 5 Ma. These ages are interpreted to date prograde metamorphism, as garnet cores are enriched in Lu compared to rims, biasing the age to early garnet growth. Pressure–temperature conditions obtained from phase equilibrium modelling are approximately 2.7 GPa and 590 °C for the lawsonite eclogite, and 2.0 GPa and 550 °C for a garnet–omphacite-bearing blueschist block within the same melange. Lu–Hf, Sm–Nd, K–Ar and Ar–Ar ages from adjacent blueschist blocks and fuchsite in serpentinite give ages between ca. 472 and 420 Ma (Fukui et al. 1995; Och et al. 2010; Tamblyn et al. 2019a). This geochronology, along with the presence of low-grade sedimentary blocks, confirms the accumulation of rocks with different *P–T* histories in the mélange.

Petrography

Mineralogy of the lawsonite eclogite block (sample RB11) has been described in detail by Tamblyn et al. (2019a) and Och et al. (2003, 2007). The eclogite contains porphyroblastic garnet, lawsonite and omphacite, in a well-foliated

matrix dominated by phengite and containing minor titanite (Fig. 2). However, it is clear from optical petrography and elemental mapping that there are two distinct mineral assemblages recorded in the sample, summarized in Supplementary Table 1, which are referred to as stage 1 and stage 2. Garnet is euhedral and forms crystals up to 7 mm in diameter, which have red-coloured cores and paler rims, referred to as garnet 1 and garnet 2, respectively (Fig. 2a–d). The inclusion relationships in garnet are summarised in Supplementary Fig. 1. Garnet 1 has inclusion-rich cores which contain lawsonite, titanite, omphacite, phengite, glaucophane, chlorite, epidote, stilpnomelane, quartz and zircon (Supp. Fig. 1). Very rarely, quartz inclusions in the outermost part of garnet 1 are surrounded by prominent radial fractures, suggesting the possibility that they were once coesite (Fig. 2e). Garnet 2 forms as ~ 400 µm wide rims on garnet 1 that contain chlorite, glaucophane, titanite, omphacite, lawsonite, quartz and zircon (Fig. 2d), and in some instances overgrow matrix phengite. Enclosed inclusions of chlorite, phengite, omphacite, quartz, titanite and pyrite occur at the boundary between garnet 1 and 2 (Supp. Fig. 1). Sigmoidal inclusion trails of titanite are also commonly truncated at the boundary between garnet 1 and garnet 2, with the trails forming at a high angle to the matrix foliation (Supp. Fig. 1). Titanite included in garnet 2 is coarser-grained than in garnet 1. Lawsonite forms euhedral crystals up to 3 mm (Fig. 2b, f). It has darker sections containing abundant fine-grained inclusions and clearer sections with coarser-grained inclusions. The inclusions are predominately titanite, epidote, glaucophane and phengite. In places, the lawsonite

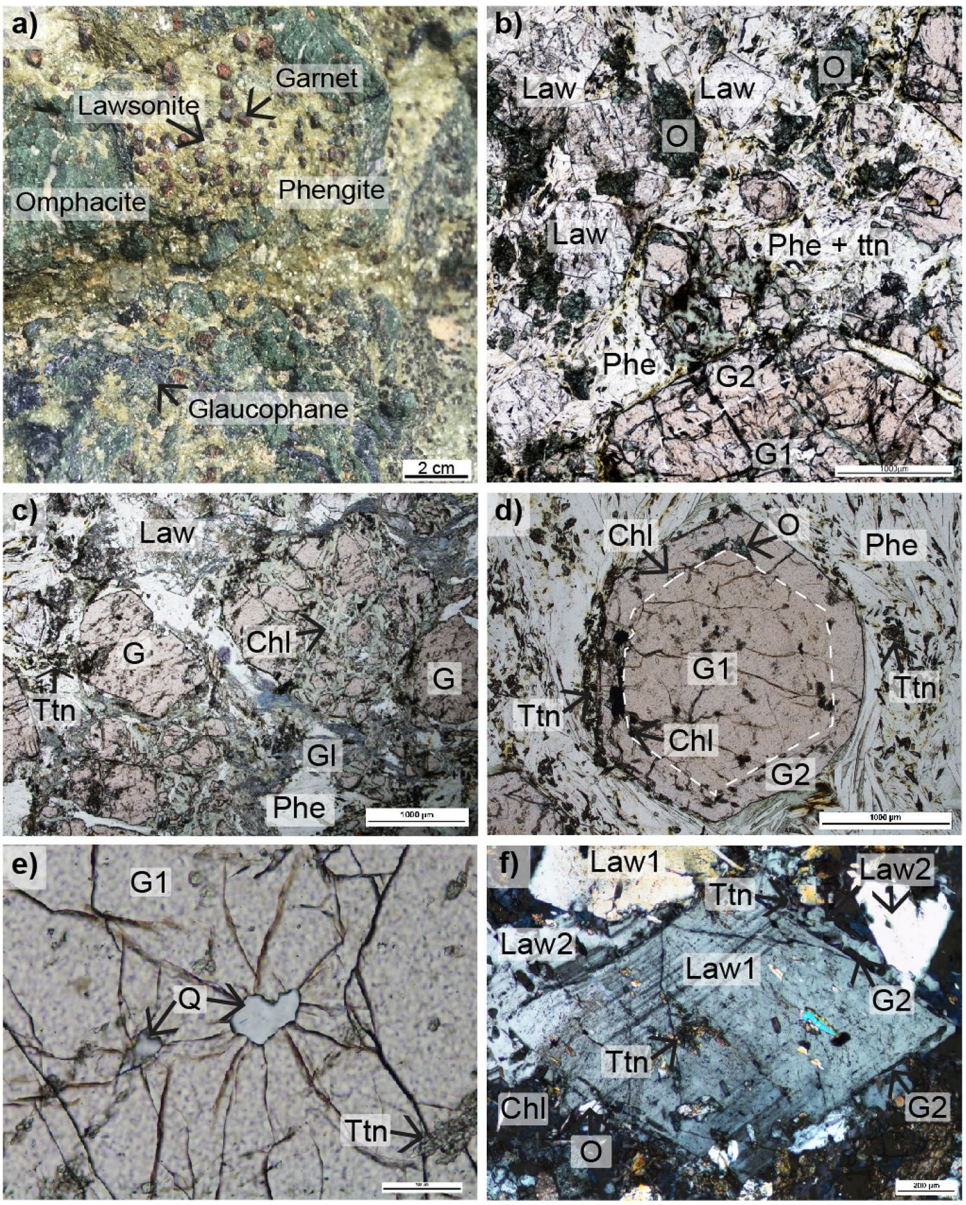

Fig. 2 Mineral textural relationships in the Port Macquarie eclogite. **a** Eclogite in outcrop, showing coarse-grained garnet, phengite and lawsonite with patches of omphacite, which is partially retrogressed by glaucophane. **b** Photomicrograph showing the porphyroblastic nature of garnet, lawsonite and omphacite, in a finer-grained phengite and titanite matrix. **c** Stage 2 retrograde features of the eclogite, showing chlorite replacement of garnet and glaucophane replacement of omphacite. **d** Garnet 2 enclosing a pre-existing garnet 1 porphyroblast. Boundary between the stage 1 garnet and stage 2 garnet is shown by a white dashed line. The boundary between the two garnet domains contains entrapped chlorite and omphacite inclusions. **e** Radial fractures surrounding a quartz inclusion in the outermost part garnet 1. **f** Large lawsonite porphyroblast, with an inclusion-rich euhedral crystal (lawsonite 1) which is overgrown by a rim (lawsonite 2). The new lawsonite growth contains inclusions of garnet 2 that developed on the margin of the older lawsonite, as well as stage 2 glaucophane and titanite. *O* omphacite, *Law* lawsonite, *Phe* phengite, *Ttn* titanate, *G* garnet, *Chl* chlorite, *Gl* glaucophane, *Stlp* stilpnomelane, *Q* quartz

grain boundaries are mantled by small garnet grains, which have been overgrown by a second generation of lawsonite. In other places, the clearer lawsonite occurs as an overgrowth on darker lawsonite crystals (Fig. 2f). The darker, older lawsonite is referred to as lawsonite 1 and the clearer overgrowths are referred to as lawsonite 2. The foliated matrix is part of the stage 2 mineral assemblage, and is defined by coarse phengite (up to 1 mm but commonly ~ 300 µm) and pervasive but modally minor titanite (< 100 µm; Fig. 2b, d). The latter is associated with fine-grained allanite and zircon (< 20 µm). Titanite and phengite are coarser in the matrix relative to the inclusions in garnet cores, and in places titanite forms aggregates of grains that rim phengite grains. Omphacite forms monominerallic patches up to 10 mm which are partially replaced by glaucophane and chlorite, as well as relic fractured porphyroblasts up to ~ 500 µm in size (Fig. 2a, b). Omphacite is partially replaced by chlorite and glaucophane. Garnet is partially replaced by chlorite along its grain boundaries or along fractures which cross-cut the garnet (Fig. 2c; Supp. Fig. 1). Where retrograde chlorite occurs with lawsonite, lawsonite is euhedral and unretrogressed, suggesting it was stable during the retrogression of the eclogite. In the matrix, glaucophane also forms foliated euhedral crystals (Fig. 2c). These crystals, as well as coarse titanite crystals, are overgrown by stage 2 lawsonite rims. These petrological observations denote two distinct stages of peak metamorphism in the eclogite, separated by a period of retrogression. A schematic representation of the petrologic observations made from optical petrography, phase mapping and elemental mapping can be found in Fig. 3.

Methods

Electron probe micro analyses and mapping

Spot analyses on minerals were obtained using a Cameca SX-5 microprobe at Adelaide microscopy, using an accelerating voltage of 15 kV and a beam current of 20 nA. Element maps used an accelerating voltage of 15 kV and a 200 nA beam current, Ca, Fe, Mn and Mg were mapped using wavelength dispersive spectrometers (WDS), whereas Al, Si, Ti, K and Na were mapped using energy dispersive spectrometry (EDS). Maps were colour scaled in ImageJ.

Phase equilibrium forward modelling

Full phase equilibrium modelling methods are in Supplementary File 1. The rock composition was calculated for the lawsonite eclogite by combining modal proportions of each mineral with its measured chemical composition (Supp. Tables 2, 3). Thin sections were mapped with a Quanta600 scanning electron microscope (SEM) with mineral liberation analysis (MLA) software to calculate modal proportions of minerals.

The phase equilibrium models were calculated using THERMOCALC (TC340i) using the internally consistent thermodynamic dataset 'ds5' (filename tc-ds55.txt; November 2003 updated version of the Holland and Powell 1998 data set) and activity–composition (a–x) models (Supp. Table 4; Holland and Powell 1988, 2003, 2011; White et al. 2007; Green et al. 2007; Diener et al. 2012) in the chemical system NCKFMASHO. A model for the local rock composition was calculated with water in excess, and a model for the local rock composition was calculated with a set water content, derived from the abundance of hydrous minerals (Supp. Tables 2, 3).

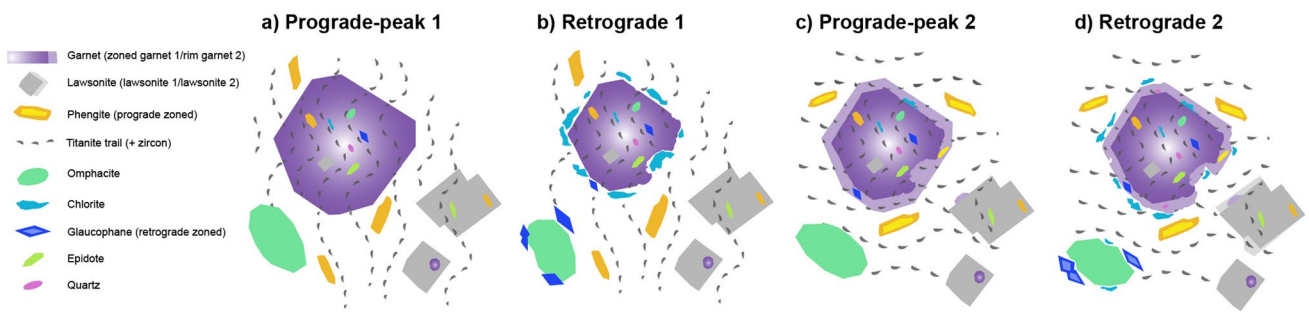

Fig. 3 Schematic interpretation of the petrologic evolution of the lawsonite eclogite. **a** Prograde-peak stage 1 burial: garnet cores nucleate and as garnet 1 grows it entraps prograde mineralogy and inclusion trails. Lawsonite porphyroblasts grow and entrap prograde minerals. **b** Retrograde 1: garnet is partially consumed by chlorite, and glaucophane forms at the expense of omphacite. **c** Prograde peak 2: garnet forms new rims (garnet 2). In rare instances, stage 2 garnet overgrows stage 1 lawsonite. Phengite recrystallises in the matrix with coarse-grained titanite during deformation. **d** Stage 2 retrograde: garnet is partially replaced by chlorite and omphacite is partially replaced by glaucophane. There is minor growth of lawsonite

U–Pb titanite geochronology

Titanite grains were analysed in situ for U–Pb isotopes using an ASI m50 LA–ICP with an attached 7700 MS at Adelaide Microscopy. Grains were ablated using a spot size of 51 µm, a frequency of 5 Hz, and a surface energy density of 3.5 Jcm^{-2}, with an acquisition time of 80 s for each analysis including 30 s of background measurement and 50 s of ablation. The primary reference titanite MKED-1 was used to correct for elemental fractionation, mass bias and instrument drift over the courses of analyses (Spandler et al. 2016), and a titanite grain from Mt Painter with an age of 442.6 ± 1.8 Ma (Elburg et al. 2003) was used as the secondary standard. Corrections were done using the software Iolite (Paton et al. 2011) and age calculations were done using IsoplotR (Vermeesch 2018). The secondary standard from Mt Painter returned a weighted mean $^{206}Pb/^{238}U$ age of 440.3 ± 2.5 Ma (MSWD = 1.5, n = 22) throughout the course of the analyses.

Ar–Ar phengite geochronology

Phengite $^{40}Ar/^{39}Ar$ isotope analyses utilized conventional furnace step-heating techniques at the University of Melbourne, after the analytical procedures of Phillips et al. (2007). Phengite grains were selected from mineral separates. Due to the possibility of contamination by excess argon in high-pressure rocks (Kelley 2002), a two-increment step-heating laser approach was employed on single grains of phengite. The laser analyses were conducted at The University of Melbourne, employing the analytical procedures described by Phillips and Harris (2008). This approach was used to screen for any significant intrasample inconsistency in argon content that could be an artefact of (i) multiple generations of phengite growth or (ii) varied amounts of isotopic resetting or excess argon contamination within single grains. Using the single-grain laser approach, spurious isotopic results from a single-grain analysis can be removed from the mean age calculations, using Isoplot software (Ludwig 2003).

Rb–Sr phengite geochronology

Phengite was analysed in situ for Rb and Sr isotopes and major and trace elements using an ESI 213 NWR (TwoVol2) laser ablation system with an attached Agilent 8800QQQ ICP-MS/MS in the Microgeochemistry Laboratory at the University of Gothenburg, Sweden, following the methods of Zack and Hogmalm (2016) and Hogmalm et al. (2017). Full methods are in Supplementary File 1. Laser parameters were a fluence of ~ 6 Jcm^{-2} and a frequency of 10 Hz. Phengite was analysed with a spot size of 40 µm, both perpendicular and parallel to cleavage. Titanite was also analysed to obtain initial $^{87}Sr/^{86}Sr$ ratios, with a spot size of 50 µm. The primary standard for $^{87}Rb/^{86}Sr$ calibration was a pressed nanopowder MicaMg ($^{87}Rb/^{86}Sr$ ratio of 154.6; Hogmalm et al. 2017). Other primary standards for $^{87}Sr/^{86}Sr$ ratios were the synthetic glass NIST610 ($^{87}Sr/^{86}Sr$ ratio: 0.709699; Woodhead and Hergt 2001) and the natural basaltic glass BCR2G ($^{87}Sr/^{86}Sr$ ratio: 0.705003; Elburg et al. 2005). Secondary standards included La Posta biotite grains, with Rb–Sr isochron age of 91.6 ± 1.2 Ma and an initial $^{87}Sr/^{86}Sr$ ratio of 0.7049 ± 5 (Zack and Hogmalm 2016), and MDC biotite grains with an isochron age of 519.4 ± 6.5 Ma and an initial $^{87}Sr/^{86}Sr$ ratio of 0.72 ± 0.002 (unpublished data). Over the course of the analyses, La Posta grains returned an isochron age of 90.5 ± 4.2 Ma, and MDC grains returned an isochron age of 501.2 ± 7.2 Ma.

LA–ICP–QQQ mapping

Phengite was mapped in situ for Rb and Sr using an ASI m50 LA–ICP–MS with attached Agilent 8800 triple quadropole MS at Adelaide Microscopy, Australia. The reaction gas used was O_2, with laser parameters of a fluence of 7 Jcm^{-2} and a frequency of 10 Hz. The primary standard used was a pressed nanopowder MicaMg, and NIST610 was used as a secondary glass standard. The maps were processed in Iolite (Paton et al. 2011). Results of the mapping are semi-quantitative, and are presented in counts per second (CPS).

Results

Electron probe micro analyses and mapping

Mineral compositions and end member proportions are reported in Supplementary Table 2 and Tamblyn et al. (2019a), additional phengite, chlorite, omphacite and glaucophane compositional data is in Supplementary Table 5.

EPMA traverses and mapping of whole garnet grains (Figs. 4, 5; Supp. Fig. 2) show complex zoning in the major elements. In garnet 1, cores show a bell-shaped Mn enrichment, consistent with prograde zoning (Figs. 4a, 5a). In the outer part of garnet 1 and prominently in garnet 2, there is a series of thin concentric Mn-rich rings or oscillations (Fig. 5b–c). These narrow Mn-rich zones are often regular, forming hexagonal garnet crystal shapes (Fig. 5c), but can also be highly irregular, appearing to form on embayments in the garnet crystal (Fig. 5b). There is an overall average increase in Mn content from the outer part of garnet 1 to the garnet 2 rim (Fig. 4b). The grossular content of the entire garnet increases slightly from core to rim, from 0.23 to 0.3, and also shows slight enrichments in thin concentric rings in the outer garnet that are correlated with the patterns exhibited by Mn (Fig. 5). Garnet 1 has almandine-poor cores

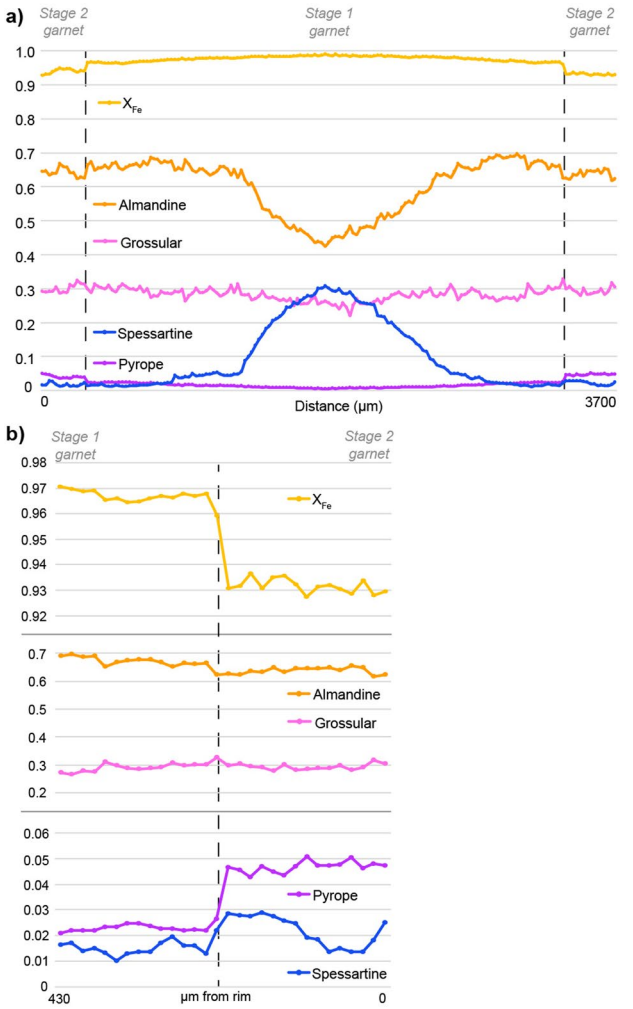

Fig. 4 Representative EPMA traverse of garnet, showing the proportions of end members and X_{Fe}. **a** Traverse across entire garnet porphyroblast, showing a prograde bell-shaped zoning profile. **b** Traverse across stage 1 garnet to stage 2 garnet, showing a step decrease in X_{Fe} and increase in spessartine content

(0.45) increasing to higher almandine content in the outer garnet (0.65; Fig. 4a), with the exception of slight almandine-poor concentric rings which correlate with the Mn-rich rings. Garnet 2 is slightly depleted in almandine (Fig. 4b). Pyrope contents are low in garnet 1, ~ 0.03, with the innermost core showing a very slight depletion compared to the rest of the garnet (Fig. 5a). Garnet 2 shows distinct step increase in pyrope (0.06) that defines an outer rim ~ 200 μm in width (Fig. 4b).

High-resolution EPMA maps (Fig. 5b–c) reveal that garnet 2 forms on a regular to irregular-shaped original surface of the garnet, as indicated by the white dashed line. The growth of garnet 2 is marked by a sharp increase in Mn, followed by several variations in Mn, and a final Mn-poor rim which has been partially replaced by chlorite. Notably, these Mn zoning patterns only correspond to slight changes in MnO (< 0.5 wt%). Fe is slightly depleted in garnet 2. This outer rim transition is also marked by a sharp increase in Mg. The oscillations in Mn commonly correlate with slight increases in Ca.

EPMA X-ray maps were also obtained from phengite grains in the matrix and in garnet (Fig. 6; Supp. Fig. 3). Matrix phengites display cores that are depleted in Fe, enriched in Al and slightly enriched in Na, surrounded by a rim enriched in Si, with enriched Fe and slight enrichment in Mg (Fig. 6). Phengite grains in garnet show phengite included in garnet 1 is enriched in Si, Mg and Fe, and depleted in Al and Na (Fig. 6). Phengite included in garnet 2 is enriched in Al and Na, and depleted in Si and Fe with a slight depletion in Mg, similar to cores of phengite grains in the matrix (Fig. 6). Compositional zoning in the phengite is sharp and well defined. Overall, the phengite zoning is defined by an increase in celadonite proportion from core (40%) to outer rim (45%), accompanied by a decrease in X_{Mg} (0.71–0.63) and an increase in Si (3.43–3.56 p.f.u.; Fig. 7).

Omphacite occurs as inclusions in garnet 1 and garnet 2, and as coarser grains in the matrix, which show subtle differences in composition (Fig. 7). Omphacite in the matrix and as inclusions in garnet 1 is generally 0.37–0.44 proportion jadeite, 0.36–0.43 proportion diopside, 0.08–0.19 proportion hedenbergite with a minor acmite component. Omphacite as inclusions in garnet 2 is similar in composition, with the exception of occasional diopsodic grains, which are 0.15–0.23 proportion jadeite, 0.47–0.50 proportion diopside, and 0.19–0.26 proportion hedenbergite. Coarse grains in the matrix and as inclusions in garnet 2 are subtly zoned in X_{Fe}, from ~ 0.27 in the core to ~ 0.23 in the rim (Supp. Fig. 4). Inclusions in garnet 1 have an average X_{Fe} of 0.28, and inclusions in garnet 2 have an average X_{Fe} of 0.3.

Chlorite forms grains in the matrix that break down garnet and omphacite, along fractures which cross-cut garnet, and as inclusions at the boundary between garnet 1 and garnet 2 (Supp. Fig. 1). Chlorite as inclusions between garnet 1 and garnet 2 has an average X_{Mg} of 0.46 (Supp. Table 5). It shows elevated MnO contents compared to the adjacent garnet (0.54–0.73 wt%). Chlorite throughout the matrix has an average X_{Mg} of 0.38. EPMA X-ray maps show that chlorite is often zoned or patchy in composition (Supp. Fig. 5).

Retrograde amphibole is ferro-glaucophane in composition after the nomenclature of Leake et al. (1997), and also shows sharply defined compositional zonation (Supp. Fig. 6). X_{Mg} increases from core to rim, accompanied by a slight decrease in Al (1.72–1.39 p.f.u.). There is a slight enrichment of Ca in the cores of the glaucophane (0.17 p.f.u.); however, the grains are dominantly sodic. Some grains have thin outer rims with slight enrichment in MnO (0.14–0.27 wt%, Supp. Fig. 6).

Titanite differs slightly from ideal formula, with incorporation of Al_2O_3 (up to 2.27 wt%), FeO (up to 0.66 wt%) and

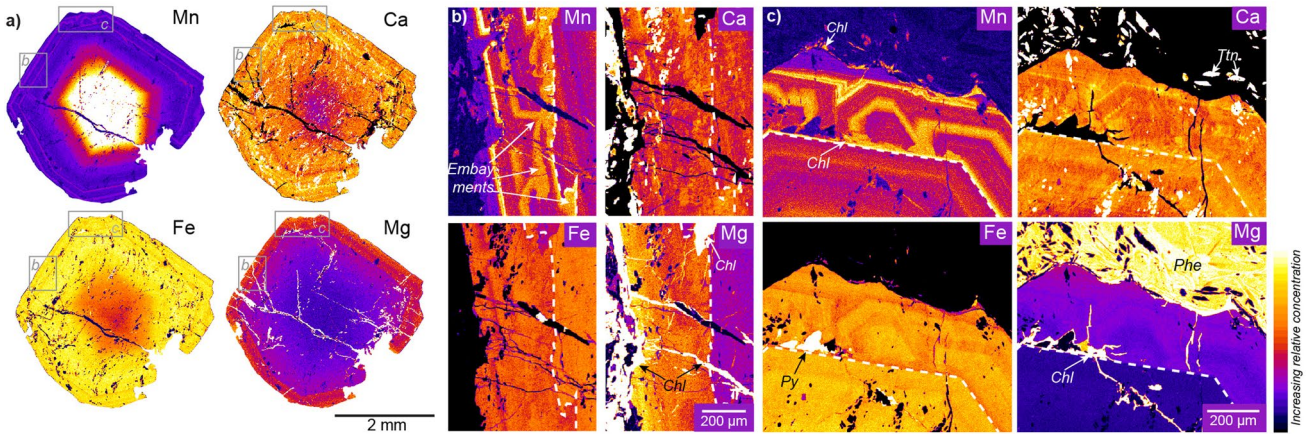

Fig. 5 EPMA element maps of garnet, the white dashed line shows the interpreted boundary between garnet 1 and garnet 2. **a** Garnet porphyroblasts with prograde zoning in Mn, along with several oscillatory rings in the stage 2 rim. Zoning in Fe and Mg show garnet 2 as a marked outer ring with elevated X_{Mg}. Subset maps are marked in grey boxes. **b** Compositional oscillations in the garnet 2 which define smaller hexagonal garnet crystals that nucleated on the older garnet 1 rim. **c** Complex Mn zoning patterns and a marked X_{Mg} increase in the outer garnet rim. Embayments and subsequent overgrowths are highlighted in the Mn oscillations, with correlate with Ca oscillations. Late chlorite replaces garnet. The boundary between garnet 1 and garnet 2 contains Mn-rich chlorite inclusions

F (up to 0.6 wt%) into its crystal structure (Supp. Table 5). Al_2O_3, FeO and F contents show positive correlations (Fig. 7).

Phase equilibrium forward modelling

The results of the phase equilibrium forward modelling and corresponding mineral modal and compositional isopleths are shown in Figs. 8, 9 and 10. Figure 8 shows the phase equilibrium model for the total bulk rock composition after Tamblyn et al. (2019a). Figure 9 shows the phase equilibrium model for the local rock composition with water in excess, and garnet 1 and lawsonite 1 removed. This was done to simulate the effective local composition for the stage 2 mineral assemblage, as garnet 1 and lawsonite 1 were chemically isolated from the reactive rock composition (e.g. Spear 1988; Marmo et al. 2002; Evans 2004; Gaides et al. 2008; Konrad-Schmolke et al. 2011; Lanari and Engi 2017). Figure 10 shows the phase equilibrium model with garnet 1 and lawsonite 1 removed, but with a set water content, calculated from the modes of hydrous minerals ($H_2O = 4.65$ wt%). This was done as the current water content in the rock is most likely a measure of the minimum amount of water available in the local rock composition. Figures 11 and 12 can only be used for the mineral relations during the secondary assemblage formation after garnet 1 and lawsonite 1 have been formed. It is likely that the local rock composition had a water content between that which is measured in the rock currently, and water in excess. Therefore, the *P*–*T* points during retrograde 1, prograde 2 and peak 2 have been interpreted from both of the models. A summary of the phase equilibrium models used for each stage of the metamorphic evolution is in Supplementary Table 6. The interpreted stages of the *P*–*T* path are indicated as grey arrows.

Stage 1

The prograde path and peak conditions for the formation of the first mineral assemblage are shown on Fig. 8b, after Tamblyn et al. (2019a). Garnet 1 nucleated at the 'garnet cores in' line at ~ 0.8–1.1 GPa and approximately 350 °C, based on the core inclusion assemblage of phengite + omphacite + lawsonite + quartz + chlorite + epidote. The path is then interpreted to track up-pressure into the + glaucophane field to satisfy the inclusion relationship of glaucophane in lawsonite and in the core domains of garnet 1 porphyroblasts.

The peak conditions of stage 1 metamorphism are determined from inclusions in the outer part of garnet 1 crystals. We acknowledge that the record of peak 1 has been obliterated by subsequent mineral growth, and as such the interpreted *P*–*T* conditions are tentative. We interpret that the lawsonite eclogite reached the phengite + garnet + lawsonite + omphacite + coesite field (based on radial fractures around quartz inclusions), at around 2.9 GPa and 600 °C. This field is bound up-pressure by the conversion of omphacite to jadeite, bound up-temperature by the destabilization of lawsonite, and is bound down-temperature and down-pressure by the loss of coesite or the conversion of coesite to quartz. No inclusions of jadeite were detected, supporting that clinopyroxene remained omphacitic during the metamorphic evolution. Lawsonite is interpreted to have been stable during stage 1 burial as lawsonite preserves ages synchronous with garnet growth (ca. 500 Ma; Tamblyn et al. 2019a), and is ubiquitously found as inclusions in garnet 1.

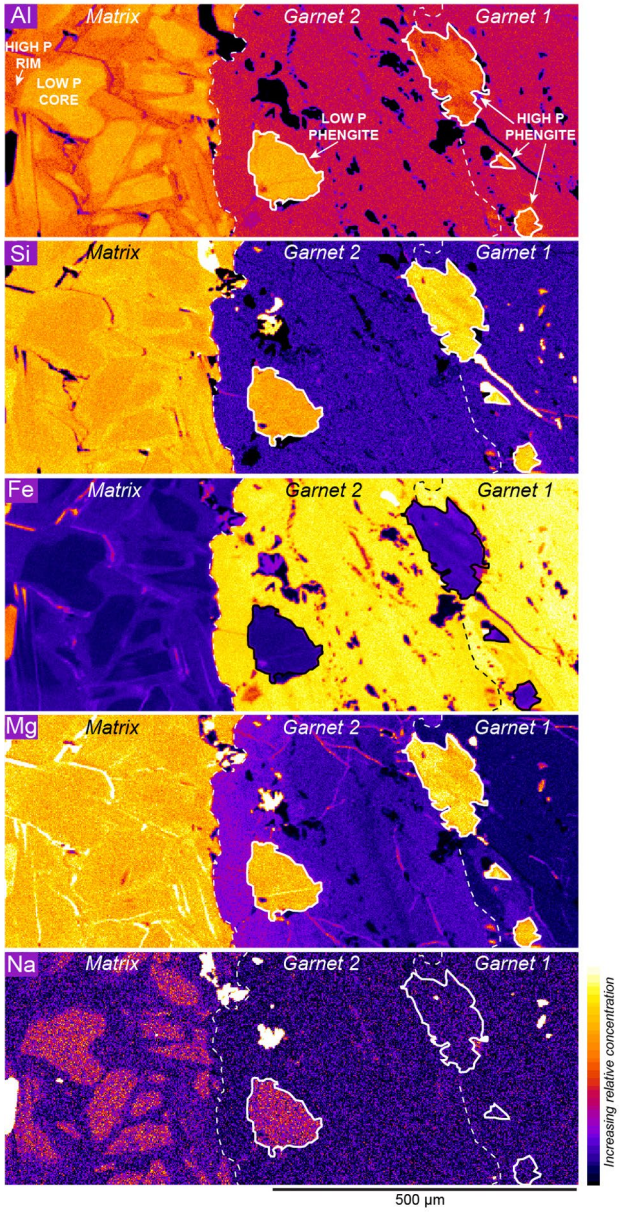

Fig. 6 EPMA maps across transition from garnet 1 to garnet 2 and into matrix phengite. White/black dashed line indicates the boundaries of garnet 1 and garnet 2. Solid white/black line indicates the boundaries of phengite included in garnet

Rare examples of radial fractures around quartz in the outer parts of garnet 1 (Fig. 2e) could indicate the former presence of coesite, further supporting these inferred *P–T* conditions.

These interpreted peak conditions are supported by the modal proportion of garnet 1. The interface between garnet 1 and 2 is marked by a step increase in X_{Mg} and a prominent increase in X_{Mn} (Figs. 4, 6), together with truncation of core-hosted inclusion trails. The microstructural relationships and change in X_{Mn} and X_{Mg} between the core and the rim strongly imply there was a hiatus in garnet growth. The overall average MnO of the garnet rim is higher than the MnO content of the outer garnet core (Fig. 4), suggesting that there was a period of garnet 1 breakdown prior to the formation of garnet 2. Making the assumption that garnet growth effectively sequesters all available MnO in the rock, particularly at high *P–T* conditions when chlorite is no longer stable, the higher average MnO concentrations in garnet 2 compared to the outer part of garnet 1 suggests that it originally occupied a larger modal proportion of the rock (Fig. 3a). The original size of the garnets during stage 1 can be calculated using the amount of MnO stored in the MnO dissolution rings in garnet 2. If the outer part of the garnet that formed during stage 1 is assumed to have had a flat MnO profile whose MnO is now incorporated into garnet 2, stage 1 garnet at one point occupied ~ 1.05 times its current modal volume, equivalent to approximately 25 mol% (1-oxide-normalised; Fig. 4a). This is a minimum estimate, as the Mn-rich garnet 2 has been partially broken down and replaced by stage 2 Mn-rich chlorite. The calculated modal proportion of stage 1 garnet porphyroblasts plots at *P–T* conditions of ~ 2.9 GPa and 600 °C (Fig. 8c), within lawsonite stability. The modal proportion of garnet at this stage of the rock's evolution may be overestimated in the phase equilibrium model, by perhaps up to 5 vol% (e.g. Lanari and Engi 2017), as garnet growth fractionates major elements. This uncertainty in the garnet mode estimate is presented on the phase equilibrium model (Fig. 8b). The calculated modal proportion of garnet passes through the phengite + lawsonite + omphacite + coesite field. The *P–T* path linking the interpreted prograde assemblages with the peak *P–T* point passes through talc-bearing *P–T* space; however, the calculated modal proportion of talc is low (< 1 vol%), and as such it is unlikely that talc would have been preserved in the eclogite.

The retrograde conditions following peak 1 must be interpreted from the phase equilibrium models calculated from the local bulk rock composition, where garnet 1 and lawsonite 1 cores are not part of the chemical system. However, the *P–T* conditions are difficult to assess, as the water content in the rock at this stage in the lawsonite eclogite's evolution is unknown. Figure 9 shows the phase equilibrium model for the local rock composition with water set to excess (i.e. water saturation), and Fig. 10 shows the same composition but with a water content defined by the current mineralogy in the rock. The amount of water currently in the rock is relevant to the assemblages formed during stage 2 retrogression; however, its relation to the assemblages formed during stage 1 retrogression is unknown. Water content affects the stable mineral assemblages at lower pressures and temperatures, particularly the stability of garnet. The primary mineralogical evidence for stage 1 retrogression is the addition of chlorite + glaucophane to the mineral assemblage (as

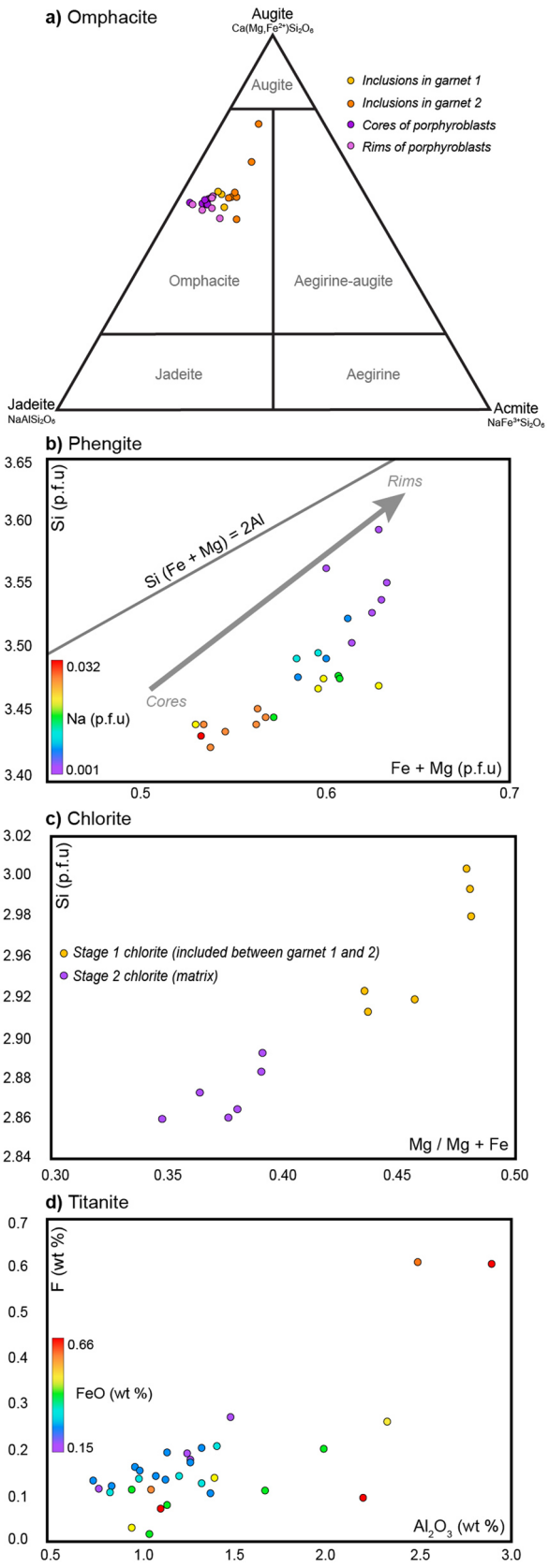

Fig. 7 Mineral compositions of omphacite, phengite, chlorite and titanite measured by EPMA. **a** Omphacite analyses from inclusions in garnet and omphacite porphyroblasts in the matrix. **b** Phengite analyses showing increasing Si, Fe and Mg component from core to rim, and decreasing Na content. **c** Chlorite analyses from stage 1 chlorite, from the boundary between garnet 1 and garnet 2, and stage 2 chlorite, from the matrix. **d** Titanite analyses showing elevated Al_2O_3, FeO and F contents with a positive correlation, suggesting increasing pressure during crystallization (e.g. Castelli and Rubatto 2002)

found as inclusions in garnet and lawsonite rims), and the consumption of garnet 1 rims. As such, the 'garnet-in' line is an important indicator of stage 1 retrograde *P–T* conditions, as it represents the modal volume of garnet in the rock before new stage 2 rims formed. In Fig. 9, the garnet-in line occurs in the retrograde assemblage at ~ 1.8–2.1 GPa and 490–500 °C. However, it is unknown if the mineral assemblage was water saturated during retrogression. If the water content was below saturation, we would expect the garnet-in line to move further down pressure and temperature. This can be seen in Fig. 10. The difference in position of the garnet-in line is due to water content limiting the formation of chlorite at the expense of garnet. Essentially, this means the garnet-in line in Fig. 9 represents the maximum pressures and temperatures the rock could have reached during stage 1 retrogression. As water saturation during retrogression seems unlikely, it appears the lawsonite eclogite may have been exhumed to lower pressures and temperatures than can be constrained. In Fig. 9, the amount of water in the local bulk composition necessary to destabilize garnet is approximately 6 wt%, 1.35 wt% more than is currently held in hydrous minerals in the rock.

Stage 2

Renewed burial leading to the growth of the new garnet rims (garnet 2) is interpreted to start at the 'garnet rims in' line (Fig. 9). This is notably only an estimate of the maximum *P–T* conditions for the start of the prograde path for stage 2, as the water content in the eclogite was unknown as this time, and it may have been exhumed to shallower conditions within the subduction channel but failed to record it. The early stages of the prograde path can be determined using compositions of the cores of stage 2 minerals. Useful compositional parameters are x(g), z(g) and y(phe), where x(g) is the X_{Fe} in garnet, z(g) is the grossular component of garnet, and y(phe) is the proportion of Al on the M2 site in phengite (i.e. dioctahedral Al), a pressure-sensitive parameter. In the *P–T* model with water in excess, the x(g) and z(g) parameters from the interior of garnet 2 plot at approximately 1.9 GPa and 500–510 °C within the prograde field. Notably, the x(phe) and y(phe) parameters from the cores of phengite intersect at approximately 2.2 GPa and 540 °C,

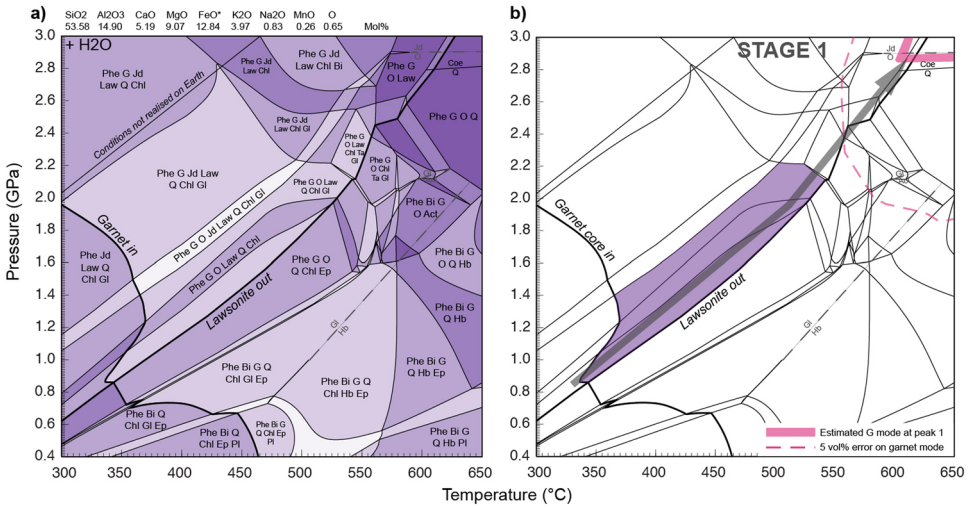

Fig. 8 **a** Phase equilibrium model calculated with THERMOCALC, modified from Tamblyn et al. (2019a), calculated with garnet 1 and lawsonite 2 included in the bulk rock chemistry. Dashed thin grey lines indicate the position of solvi. Colour changes indicate changes in variance across fields. **b** Model **a** showing the prograde assemblage and estimated garnet mode at stage 1 peak. Thick grey arrow indicates the interpreted *P–T* path of stage 1 prograde peak. *Act* actinolite, *Bi* biotite, *Chl* chlorite, *Coe* coesite, *Ep* epidote, *G* garnet, *Gl* glaucophane, *Hb* hornblende, *Jd* jadeite, *Law* lawsonite, *O* omphacite, *Pa* paragonite, *Phe* phengite, *Pl* plagioclase, *Q* quartz, *Ta* talc

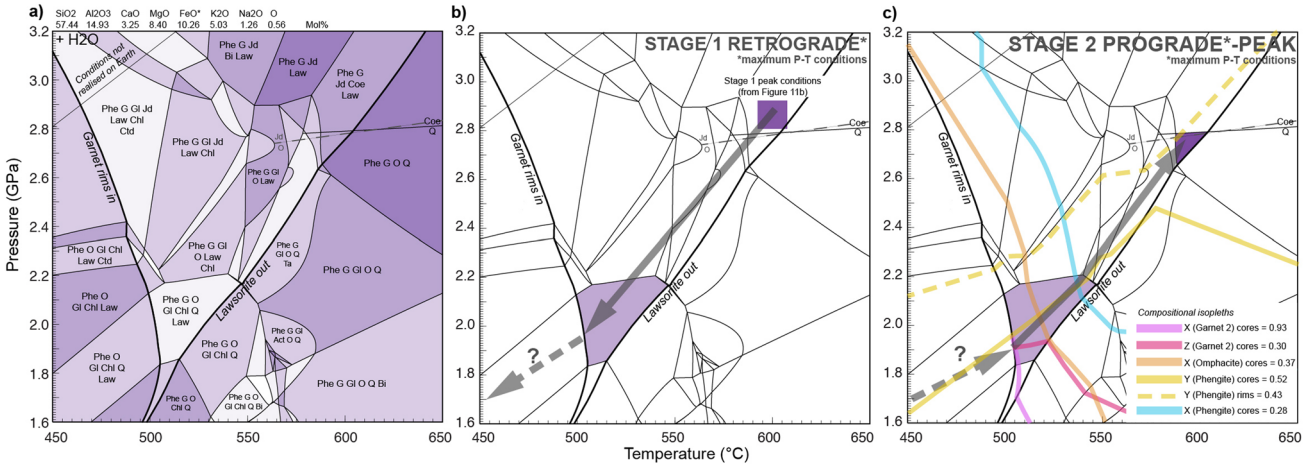

Fig. 9 **a** Phase equilibrium model calculated with THERMOCALC for the local rock composition with garnet 1 and lawsonite 1 removed, and water in excess. Dashed thin grey lines indicate the position of solvi. Colour changes indicate changes in variance across fields. Note the scale change from Fig. 8. **b** Model **a** showing the interpreted peak conditions of stage 1 peak from Fig. 8b, and the interpreted stage 1 retrograde path in the thick grey arrow. Note these retrograde *P–T* conditions are considered the maximum possible pressures and temperatures obtained during retrogression. **c**) Model **a** showing the interpreted stage 2 prograde and peak assemblages, and mineral compositional isopleths. Thick grey arrow indicates the interpreted *P–T* path during stage 2 prograde to peak. Abbreviations are listed in Fig. 8

possibly indicating the initiation of recrystallisation of phengite at this *P–T* point. The *x*(o) parameter from cores of omphacite grains, which reflects the X_{Fe}, also plots close to these conditions, however, as the textural timing of omphacite growth in this sample is not well known, it is not clear if its compositions reflect stage 1 burial or stage 2 burial. In the *P–T* model with set water content, these same compositional parameters plot over a larger range of *P–T* conditions; however, converge towards 1.95 GPa and 450 °C. The *x*(phe) and *y*(phe) parameters from the cores of phengite intersect at the same point as Fig. 9: 2.2 GPa and 540 °C. As such, an alternative prograde 2 *P–T* path may have begun at lower pressures and temperatures and tracked up towards ~ 2.2 GPa and 540 °C.

The peak assemblage during stage 2 is interpreted to have been phengite + garnet + omphacite + lawsonite + quartz,

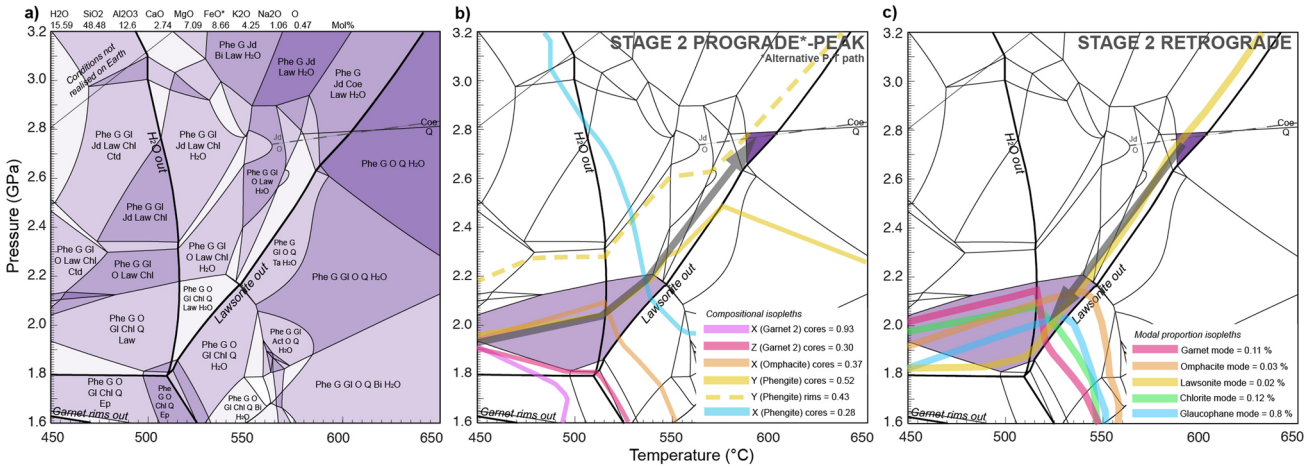

Fig. 10 **a** Phase equilibrium model calculated with THERMOCALC for the local rock composition with garnet 1 and lawsonite 1 removed, and set water content. Dashed thin grey lines indicate the position of solvi. Colour changes indicate changes in variance across fields. Note the scale change from Fig. 8. **b** Model **a** showing a possible alternative path for stage 2 prograde, based on compositional isopleths from garnet 1, omphacite and phengite cores. Peak conditions remain the same. **c** Model **a** showing the final stage 2 retrograde conditions reached, based on modal proportion isopleths. Abbreviations are listed in Fig. 8

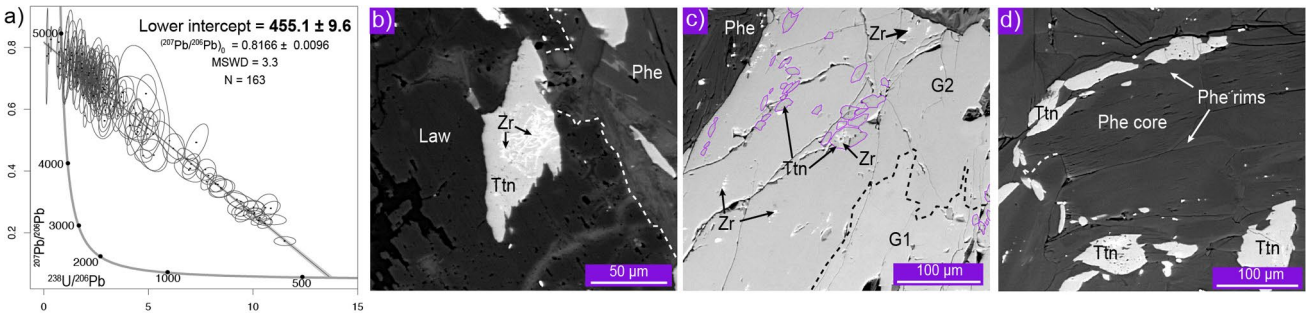

Fig. 11 Results of LA–ICP–MS U–Pb titanite geochronology and representative BSE images of analysed titanite grains. **a** Terra–Wasserburg plot. **b** Coarse-grained titanite in the rim of a stage 2 lawsonite crystal (outlined in white dotted line) displaying a well-formed mesh-like intergrowth of exsolved zircon. **c** Coarse titanite trails outlined in purple in the rims of stage 2 garnet, which is distinguished from the stage 1 garnet core by the black dotted line. **d** Titanite grains rim a prograde-zoned phengite, which has darker cores and brighter rims

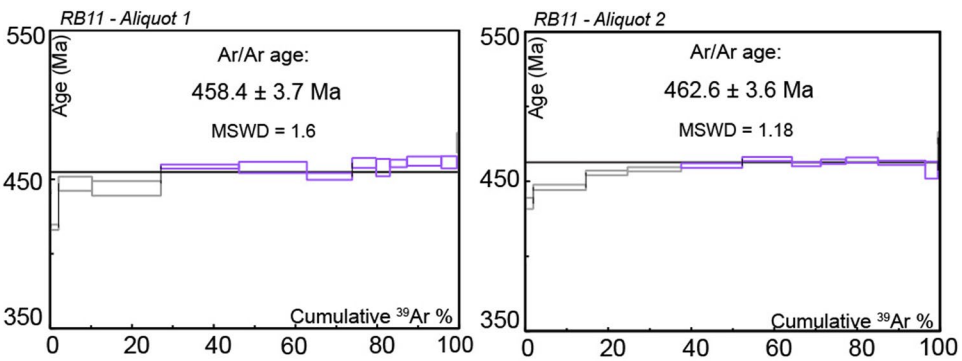

Fig. 12 Step-heating Ar–Ar results from two phengite grains in the lawsonite eclogite

which is modelled to occur at conditions of ~ 2.7 GPa and 590 °C. This field exists identically on both Figs. 9 and 10, and is bound up-temperature by the loss of lawsonite, down-temperature by the presence of talc and/or glaucophane, and up-pressure by the conversion of quartz to coesite and/or omphacite to jadeite.

Stage 2 retrograde *P–T* conditions are constrained from Fig. 10. It is characterised by the growth of chlorite and retrograde-zoned glaucophane at the expense of garnet and omphacite. It also includes a modal proportion increase in lawsonite (lawsonite 2), which overgrows garnet 2 (Fig. 2f). The current modal proportions of all stage 2 minerals—minus the garnet 1 and lawsonite 1 cores which are not included in the modelling—intersect in the phengite + garnet + lawsonite + omphacite + quartz + chlorite + glaucophane + H_2O field (Fig. 10c). The modelled isopleths track parallel to each other down temperature in the H_2O absent field, spanning between 1.8 and 2.1 GPa (Fig. 10c). Final recorded retrogression is, therefore, interpreted to occur down to ~ 2.0 GPa and 520 °C.

U–Pb titanite geochronology

In situ U–Pb isotopic analyses of titanite in the matrix and in the garnet 2 rims define a common lead trend with a lower intercept of 455.1 ± 9.6 Ma (MSWD = 3.3, n = 163, Fig. 11a). The upper intercept has a $^{206}Pb/^{207}Pb$ ratio of 0.8166 ± 0.0096. During data processing, 16 analyses were discarded due to low or no signal, and a further 23 analyses were discarded due to contamination from detectable or visible microzircons. Incidental ablation of these zircons was visible in the signals as large Zr spikes. U–Pb geochronological data can be found in Supplementary Table 7.

Ar–Ar phengite geochronology

Step-heating results of two aliquots of phengite from the lawsonite eclogite taken from ~ 50 cm apart are shown in Fig. 12. The mineral grains come from the rock matrix. Ar–Ar data can be found in Supplementary Table 8. For aliquot 1, an age of 458.4 ± 3.7 Ma was obtained from 72.4% of released ^{39}Ar. Aliquot 2 shows a rise in age with increasing temperature steps. An age of 462.6 ± 3.6 Ma was calculated from 61.9% of released ^{39}Ar.

Rb–Sr phengite geochronology

In situ LA–ICP–MS Rb–Sr analyses of phengite cores and rims produce almost identical isochrons (Fig. 13). Phengite rims have a wide range of $^{87}Rb/^{86}Sr$ ratios and produce an age of 448 ± 13 Ma (MSWD = 0.61, n = 18, Fig. 13a), in many cases with favourably high $^{87}Rb/^{86}Sr$ ratios (up to 2000). Phengite cores generally have lower $^{87}Rb/^{86}Sr$ ratios and produce an age of 437 ± 37 Ma (MSWD = 0.84, n = 16, Fig. 13b). When combined, all phengite data give an isochron age of 449 ± 19 Ma (MSWD = 0.55, n = 34, Fig. 13c). Based on textural evidence that titanite occurs as inclusions in phengite, as matrix grains and locally as grains rimming phengite (Fig. 11), it was assumed to have grown synchronously with matrix phengite. Therefore, titanite was analysed to obtain an initial $^{87}Sr/^{86}Sr$ ratio to anchor the isochron, producing an average $^{87}Sr/^{86}Sr$ ratio of 0.70986 (n = 6, Fig. 13d). The rims are interpreted to form during peak metamorphism and thus were used in the final age calculations. When the phengite rims are anchored with the titanite analyses, the isochron age produced is 450 ± 11 Ma (MSWD = 1.09, n = 26, Fig. 13e). Rb–Sr geochronological data can be found in Supplementary Table 9.

LA–ICP–QQQ isotope mapping

Phengite was mapped for ^{85}Rb and ^{87}Sr (Fig. 14). The qualitative results reveal the phengites that are zoned, showing enrichments in Sr in the cores of the grains with slight Rb depletion, and Rb enrichments in the rims which correlates to comparatively low levels of Sr. The boundary between these cores and rims is sharp, and in larger grains is aligned along cleavage (Fig. 14). This zoning correlates to zoning seen in the major elements; Sr-enriched cores correspond to low-Si/high-Al cores, and Rb-enriched rims correspond to high-Si/low-Al rims. High-Sr grains are titanite. The outline of phengite grains is shown in white.

Discussion

Petrological evidence for reburial of the lawsonite eclogite

Petrographical observations from the block of lawsonite eclogite in the Port Macquarie serpentinite melange denote at least two interpretable burial events, summarized in Supplementary Table 1 and schematically outlined in Fig. 3.

Evidence for stage 1 prograde (or burial 1) is preserved in the cores of garnet porphyroblasts, which are prograde zoned, showing bell-shaped Mn profiles. Lawsonite porphyroblasts grew in equilibrium with garnet, as evidenced by their ca. 500 Ma age, synchronous with garnet growth (Tamblyn et al. 2019a). Stage 1 burial is also recorded by phengite inclusions in the outer part of garnet 1, which are high in Si and low in Al, consistent with crystallization at high pressure. It is possible that rare coesite was formed and captured in the outer parts of garnet 1, interpreted from the presence of radial fractures around quartz.

The petrologic evidence for a second burial event after partial exhumation is recorded as inclusions within garnet rims, lawsonite rims, and the compositions of matrix minerals. The step increase in X_{Mg} and a Mn oscillation marks the boundary of new garnet 2 growth, and the general increased Mn throughout the new garnet rim suggests that it was formed from the breakdown of previously larger garnet porphyroblasts. The presence of chlorite on the boundary

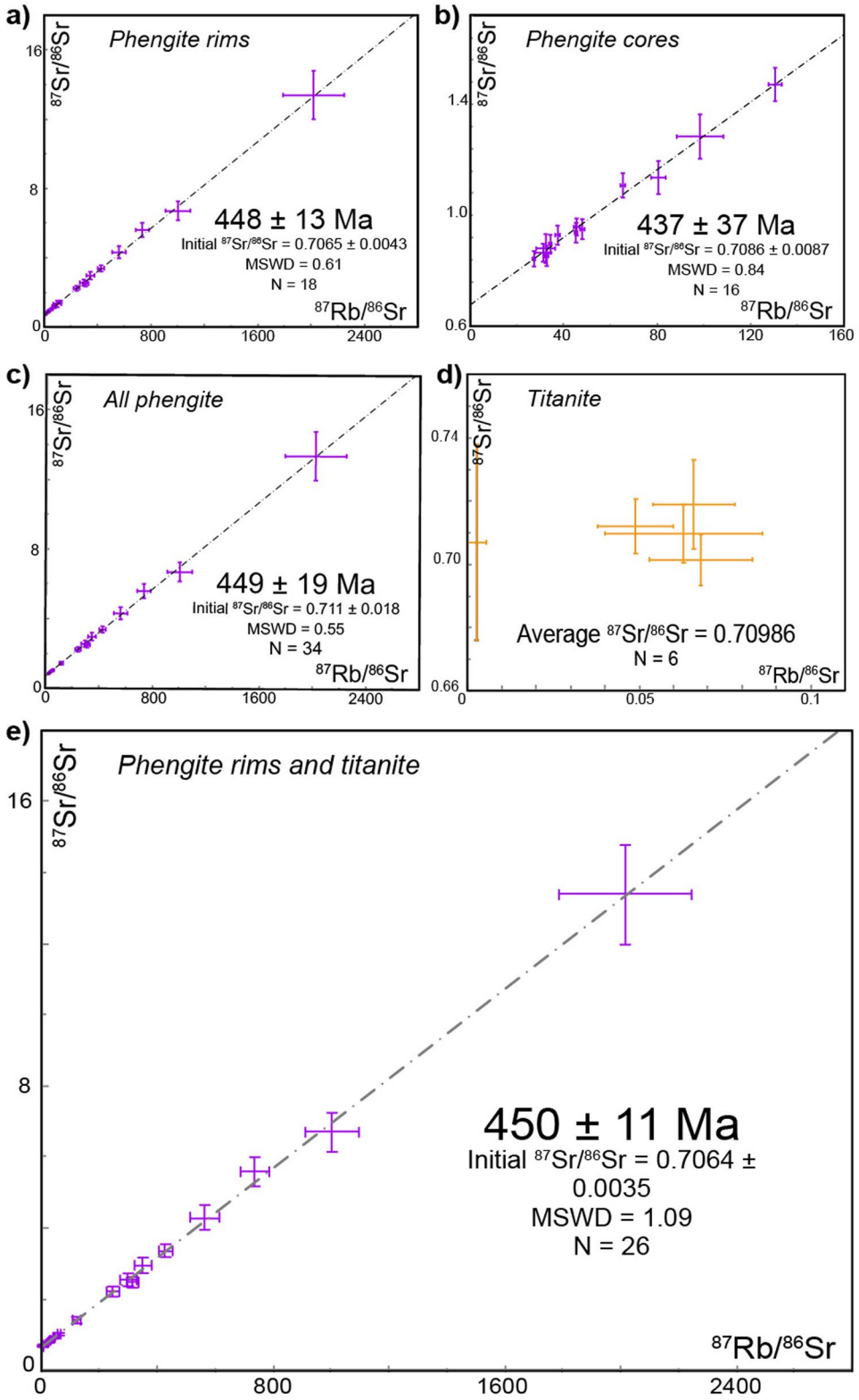

Fig. 13 In situ LA–ICP–MS Rb–Sr geochronological results. **a** Isochron constructed from analyses of phengite rims. **b** Isochron constructed from analyses of phengite cores. **c** Isochron using both phengite cores and rims. The isochrons produce similar ages within the uncertainties. **d** Isotopic analyses of texturally intergrown titanite, which records the initial $^{87}Sr/^{86}Sr$ isotopic ratio. **e** Isochron constructed from phengite rims and anchored with titanite analyses

between garnet 1 and garnet 2 is key evidence that lower temperatures and pressures were reached before the growth of garnet 2. Omphacite grains in the matrix are prograde zoned (Supp. Fig. 4), and possibly grew from the breakdown of glaucophane during the second burial event, however, may also be relic from stage 1. Phengite and titanite (which make up the strongly foliated rock matrix) underwent recrystallization during prograde 2 deformation (e.g. Spencer et al.

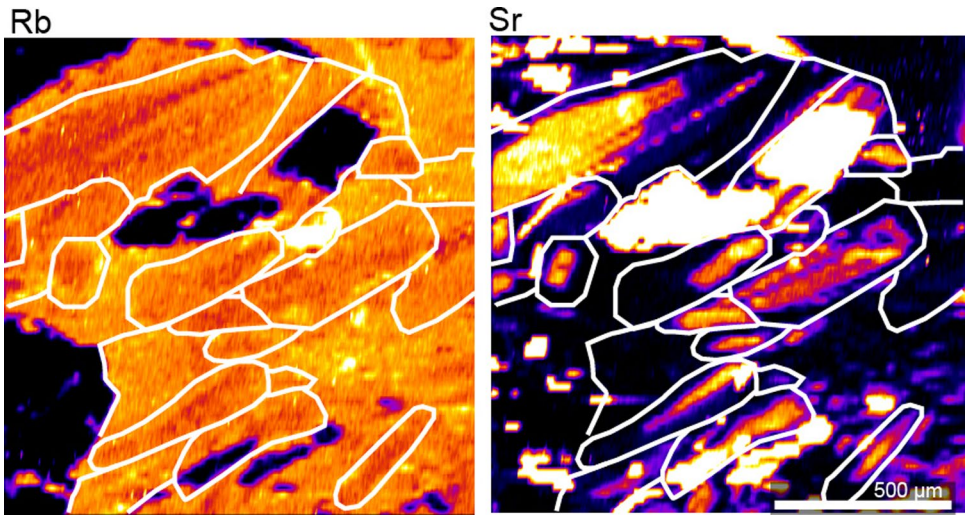

Fig. 14 LA–ICP–MS Rb and Sr maps of phengite from the lawsonite eclogite. Maps are semi-quantitative. Phengites show Sr enrichments of all isotopes in their cores, and sometimes a slight Rb enrichment in their rims. These enrichments follow along cleavage planes of the phengite. The boundaries between these rims and cores are extremely sharp and well defined. The Sr-rich mineral is titanite. The outline of phengite grains is shown in white. Rb-rich material without obvious grain boundaries traced is fine-grained phengite

2013; de Meyer 2014; Itaya and Tsujimori 2015). This interpretation is supported by petrological observation that the pervasive foliation in the matrix is at an oblique angle to the foliation preserved as inclusion trails in garnet 1 (Fig. 3c). The prograde zoning in the phengite is consistent with recrystallization with increasing pressure and temperature; however, the sharp boundary between zones could either be interpreted as (i) progressive prograde zoning during total recrystallization of the phengite grains or (ii) partial recrystallization of the phengite rims at higher pressure, preserving an older low-pressure core. Phengite with low Si/high Al, identical to the cores of phengite in the matrix, is preserved in the garnet 2 rims (Fig. 6), providing further evidence that garnet 2 rims grew at lower *P–T* conditions than the outer parts of garnet 1. Evidence for stage 2 retrograde includes partial replacement of garnet by chlorite, and partial replacement of omphacite by glaucophane and chlorite (Fig. 3d). Retrograde zoning in glaucophane (Supp. Fig. 6) supports that it grew during decreasing pressure and temperature. New lawsonite growth on existing crystals captured coarse titanite, garnet and glaucophane, suggesting that lawsonite increased its modal proportion during retrograde 2 (Fig. 3d).

The origin of oscillatory garnet zoning and the possible role of fluids

Garnets from the lawsonite eclogite show oscillatory zoning in Ca, Mn, Fe and Mg (Fig. 5; Supp. Fig. 2), which is subtle in the outer parts of stage 1 garnet but marked throughout the stage 2 garnet rims. Narrow annuli enriched in Mn and Ca are depleted in Fe and Mg, and vice versa. The oscillations are sharp; they occasionally form epitaxial hexagonal crystal shapes on pre-existing garnet (Fig. 5c), or form on irregular-shaped embayed surfaces of pre-existing garnet (Fig. 5b). These features suggest that garnet was resorbed and regrown several times during the metamorphic history of the lawsonite eclogite (aside from the major garnet resorption event between burial 1 and burial 2).

Garnet resorption and regrowth have been suggested to occur via changes in pressure and temperature which influence garnet stability (e.g. García-Casco et al. 2002; Kohn 2004). This mechanism has been interpreted as the cause of oscillatory garnet zoning from high-pressure rocks in subduction systems, where seismic instability and/or serpentinite hosted channel circulation cause cyclic *P–T* changes (García-Casco et al. 2002; Li et al. 2016; Viete et al. 2018). However, garnet resorption has also been suggested to be a result of external fluid influx, which dissolves and reprecipitates garnet in equilibrium with the fluid (Angiboust et al. 2011; Hyppolito et al. 2019). Additionally, the influx of fluids may enrich or deplete cations incorporated into the garnet during its growth (e.g. Martin et al. 2011; Angiboust et al. 2014; Park et al. 2017). Such fluid influxes may not be easy to trace; however, the lack of oscillatory zoning in the major elements of other minerals (e.g. phengite, omphacite) suggests that fluid influxes did not occur on a major scale, or at least were only recorded in garnet. As there is no petrologic evidence supporting either case, the major element oscillatory zoning in garnet is interpreted to have formed by subtle fluctuations in *P–T* and/or influxes of fluid.

P–T conditions of reburial

The record of the *P–T* conditions during the first burial event is contained as inclusions in lawsonite and garnet, while the record of the second burial event is found in garnet and lawsonite rims and the matrix mineralogy. The *P–T* path proposed is summarised in Fig. 15, the interpreted conditions are summarised in Supplementary Table 6. The proposed *P–T* path is tentative, due to the difficulty in reconstructing the mineralogical evolution of the sample.

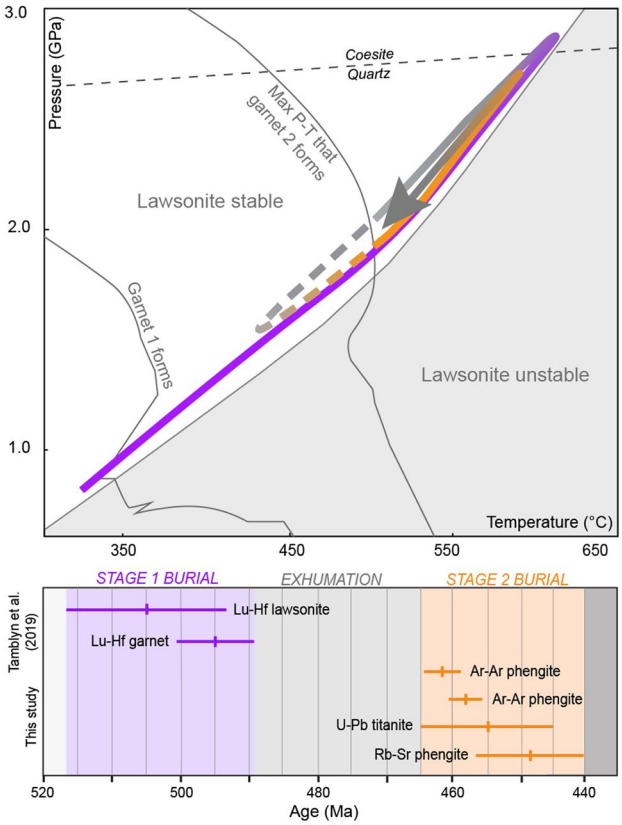

Fig. 15 Summary of the *P–T–t* path of the lawsonite eclogite. Lu–Hf geochronology from lawsonite and garnet dates an earlier event during burial 1. Ar–Ar and Rb–Sr data from phengite, and U–Pb data from titanite, date a younger recrystallization event associated with reburial of the lawsonite eclogite within the subduction channel. This results in two hairpin *P–T* loops. While the exact timing of exhumation and *P–T* conditions reached between these two burial events is unknown, it must have occurred between approximately 485–465 Ma

The *P–T* path during stage 1 burial is recorded from 0.8 to 1.1 GPa at approximately 350 °C, and then tracks up to peak conditions of at least 2.9 GPa and 600 °C based on lawsonite stability, inclusion assemblages in lawsonite and garnet and the estimated modal proportion of garnet (Fig. 8). The potential former presence of coesite, now recorded by radial fractures around quartz inclusions in the outer parts of garnet 1, supports these peak conditions. High-Si/low-Al phengite inclusions in the outer parts of garnet 1 also support that high pressures were reached during this stage (Fig. 6). Subsequent retrogression to maximum conditions of ~ 2.0 GPa and 500 °C is recorded by the consumption of garnet, and growth of chlorite and glaucophane (Figs. 9, 10). It is likely the lawsonite eclogite reached lower pressures and temperatures than this during retrogression; however, this part of its evolution is difficult to reconstruct.

Stage 2 reburial began at maximum conditions of ~ 2.0 GPa and 500 °C. Growth of new garnet rims with elevated Mn and X_{Mg} captured the stage 1 chlorite and glaucophane. Stage 2 peak conditions of 2.7 GPa and 590 °C were reached, based on the preserved peak mineral assemblage. Retrogression to approximately 1.9 GPa and 520 °C is based on the current modal mineralogy of the rock (Fig. 10c), and is supported by the formation of retrograde-zoned glaucophane and the partial break down of garnet to form chlorite.

If these tentative estimates are taken at face value, the earliest stages of the prograde evolution of the rock occurred on a geothermal gradient of approximately 370 °C/GPa, while the peak and retrograde stages of both stage 1 and 2 occurred on a cooler geothermal gradient of approximately 210–265 °C/GPa. These gradients are in line with a subduction channel which is cooling over time, potentially in response to the refrigeration effects of ongoing subduction (Gerya 2002; Agard et al. 2018). If this is correct, it suggests the eclogite records the transition from subduction initiation (e.g. Tamblyn et al. 2019a) to subduction maturity. These inferred geothermal estimates are comparable to the geothermal gradient experienced by garnet blueschist from the same mélange that hosts the lawsonite eclogite at Port Macquarie (~ 275 °C/GPa; Tamblyn et al. 2019a). The complete *P–T* path suggested in Fig. 15 is two hairpin loops, which are constrained by the presence of lawsonite throughout the recorded history. Such *P–T* evolutions have been previously suggested for high-pressure rocks in oceanic subduction systems (e.g. Gerya et al. 2002; Krebs et al. 2011; Pourteau et al. 2019).

Timing of reburial

Tamblyn et al. (2019a) obtained Lu–Hf ages of 489.7 ± 5 Ma for garnet whole rock and 505 ± 15 Ma for lawsonite whole rock from the eclogite. The cores of stage 1 garnet are highly enriched in Lu compared to the stage 2 garnet, indicating the garnet Lu–Hf age is essentially the age of stage 1 garnet growth. The lawsonite Lu–Hf age is less precise but within uncertainty of the garnet age, suggesting that stage 1 garnet and stage 1 lawsonite grew within a single isotopic reservoir at ca. 500–490 Ma. The lawsonite grains contain patches that are enriched in Lu (Tamblyn et al. 2019a), and in places are overgrown by volumetrically minor second generation lawsonite (Fig. 2f). The Lu-rich domains in stage 1 lawsonite formed prior to garnet nucleation. The *P–T* path during the stage 1 burial tracks up to tentative peak conditions of at least 2.9 GPa and 600 °C ("*P–T* conditions of reburial"). This occurred at ca. 505–490 Ma as dated by garnet and lawsonite Lu–Hf (Tamblyn et al. 2019a; Fig. 15).

Matrix phengite that encloses garnet, lawsonite and omphacite porphyroblasts shows an increasing Si and celadonite content from core to rim (Fig. 6; Carswell et al. 2000). This compositional component is consistent with increasing pressure, which in the absence of information

about changes in non-lithostatic stress, equates to increasing burial depth. The plateau ages obtained from Ar–Ar geochronology from phengite from the rock matrix give ages of ca. 458 and ca. 462 Ma. The suggested closure temperature of argon diffusion in phengite is variable (e.g. Warren et al. 2011; Fornash et al. 2016), and is dependent on grain size and fluid availability (e.g. Glodny et al. 2002). Numerical diffusion modelling suggests that phengite grown at blueschist to eclogite facies (up to 550 °C) can retain argon from its prograde history (Warren et al. 2011). This has been supported by step-heating experiments which suggest phengite can be highly retentive of argon (Forster and Lister 2014). These findings are in line with samples from high-pressure terranes where Ar–Ar ages are similar to peak metamorphic ages obtained from zircon or garnet geochronology (Fornash et al. 2016), or can be texturally related to mineral growth during sequential phases of deformation (Putlitz et al. 2005).

In situ LA–ICP–MS Rb–Sr dating of mica is still in its infancy as a geochronological technique. However, it has the potential to rapidly constrain ages of metamorphism and deformation in metamorphic rocks. Rb–Sr analyses of phengite rims, coupled with an initial $^{87}Sr/^{86}Sr$ value from texturally intergrown titanite, give an isochron age of ca. 450 Ma. The rims of phengite were selected for the final age calculation, as they are interpreted to grow at peak conditions of stage 2.

Rb and Sr maps also support that the geochronologic results are growth ages (Fig. 14); the zoning is sharply defined, suggesting minimal post-growth diffusion within the grains (e.g. Konrad-Schmolke et al. 2011). Rb–Sr maps show Sr enrichments in the low-Si cores of phengite, and Rb enrichments in the high-Si rims, a pattern that has been noted in high-pressure rocks (Di Vincenzo et al. 2006). The incorporation of Sr into phengite may, therefore, be related to the breakdown of another Sr-bearing mineral in the system at lower pressures, or, a preference for Sr in low-Si less-phengitic white mica, which declines with increasing phengitic component up-pressure. The Rb–Sr age of the phengite rims is within uncertainty of the age obtained from phengite Ar–Ar analyses and titanite U–Pb age of ca. 455 Ma (below). This interpretation is in line with similar high-pressure terranes, where Rb–Sr dates record crystallization of phengite on the prograde-peak path during metamorphism (e.g. Hetzel and Romer 2000; Glodny et al. 2002; Bosse et al. 2005; Di Vincenzo et al. 2006). In some of these examples, Rb–Sr phengite growth ages are synchronous with Ar–Ar phengite ages (Anczkiewicz et al. 2000; Hetzel and Romer 2000; Glodny et al. 2002; Rodríguez et al. 2003). Rb–Sr has also been shown to date continuous recrystallization of white mica during retrograde deformation in polymetamorphic terranes, at peak temperatures of ~ 500–550 °C (Bröcker et al. 2013), demonstrating the ability for the Rb–Sr white mica ages to record recrystallization events.

The U–Pb data from titanite in the matrix and as inclusions in the stage 2 garnet gives an age of ca. 455 Ma. Although there is some dispersion in the data, it is evident the matrix titanites are significantly younger than the ca. 490 Ma age for stage 1 lawsonite and garnet. Phase equilibrium modelling suggests the rock experienced *P–T* conditions below the closure temperature of titanite (~ 600–800 °C; Hartnady et al. 2019). Additionally, there is no evidence of a rutile-bearing assemblage in the lawsonite eclogite. Therefore, it is unlikely the titanite formed from breakdown of rutile on the retrograde path. Consequently, we interpret the titanite U–Pb data to reflect the timing of titanite recrystallisation.

Titanite occurs throughout the matrix and forms around the edges of prograde-zoned phengite (Fig. 11b–d). It occurs as fine-grained inclusion trails in garnet cores and lawsonite, and as coarse-grained inclusions in stage 2 garnet and lawsonite rims (Fig. 11b–c). These textural relationships indicate that titanite was stable during the entire metamorphic evolution of the eclogite, first growing during the stage 1 burial event, and recrystallizing during the prograde evolution of the stage 2 burial event to form coarser-grained titanite. This recrystallization was possibly tracked by increasing F, Al_2O_3 and FeO content in the titanite (Fig. 7).

The inclusions in titanite are limited to fine-grained apatite, phengite and zircon (< 10 µm). Zircon is either euhedral and 5–10 µm in size, or occurs as fine-grained clusters or web-like intergrowths which are 2 µm or less (Fig. 11b, c). The 5–10 µm sized apatite, phengite and zircon inclusions are interpreted to predate the crystallization of titanite, and were avoided during analyses. However, the extremely fine-grained web-like microzircon was difficult to avoid, and was possibly incorporated into analyses. This is suggested by Zr concentrations in the titanite analyses of up to ~ 18,800 ppm (Supp. Table 7). Texturally, these extremely fine-grained zircon dustings only occur in sections of titanite grains, and are absent in phengite, garnet, lawsonite and omphacite. This suggests they are probably exsolution of Zr from the titanite, rather than inclusions (Fig. 11b, c). Titanite can substitute Zr^{4+} for Ti^{4+} in its crystal lattice, as evidenced by development of the Zr-in-titanite thermobarometer (Hayden et al. 2008). However, in quartz-absent rocks, titanite can take in significant amounts of ZrO_2 (up to 15 wt%; Della Ventura et al. 1999; Seifert and Kramer 2003; Seifert 2005; Vuorinen and Hålenius 2005; Liferovich and Mitchell 2005; Chakhmouradian 2004). While these studies are from igneous rocks, they demonstrate the ability for significant Zr to substitute into titanite.

The phase equilibrium modelling of the stage 2 effective bulk composition suggests the prograde-peak path taken by the lawsonite eclogite during reburial was quartz free until absolute peak conditions were obtained (590 °C, 2.7 GPa). Zircon exsolution from titanite has not been directly reported

before, but in lieu of other explanations, we suggest these fine-grained clusters of zircon within titanite represent high-Zr titanite which formed in a quartz-absent matrix assemblage, which then exsolved zircon after crystallization of the parent mineral. As such, while we tried to avoid areas of obvious web-like zircon in titanite, we suggest that if small amounts of fine-grained zircon exsolution were incorporated into the titanite U–Pb analyses, we are dating U–Pb isotopic ratios related to titanite recrystallization at ca. 455 Ma.

The above interpretations suggest recrystallization of phengite and titanite at ca. 450 Ma dates the timing of burial 2, which reached peak *P–T* conditions of 2.7 GPa and 590 °C. The two burial events were separated by a period of exhumation to maximum conditions of approximately 2.0 GPa and 500 °C, however the lawsonite eclogite may have been exhumed further up the subduction channel. The two stages of metamorphism and burial in the lawsonite eclogite occurred over a period of at least ca. 50 M y (Fig. 15). The timing of final exhumation after burial 2 is unknown, but had occurred by the Permian, based on serpentinite detritus in nearby early Permian basins in the SNEO (Aitchison et al. 1994).

Examples of other burial cycles

The suggestion that the block of lawsonite eclogite at Port Macquarie underwent two stages of burial, each marked by garnet growth and separated by a stage of garnet breakdown, is similar to *P–T* histories proposed from other studies on subducted rocks in oceanic settings, and is supported by results of numerical modelling (e.g. Gerya et al. 2002). Despite the difficulties in recognizing and constraining multiple cycles of burial and exhumation within single high-pressure samples, workers have had success using various geochronological and mineralogical tools. Dating zones within metamorphic zircon, combined with REE chemistry and inclusion assemblages, have allowed two or more subduction cycles to be identified in Rhodope, Greece (Liati et al. 2016) and the Italian Alps (Rubatto et al. 2011); however, the latter was within a continental subduction system. Three burial cycles in the Sambagawa belt in Japan have been identified from mineral assemblages and mineral chemistry of garnet and amphibole in eclogite by Kabir and Takasu (2010). Two burial cycles are recorded in eclogite from the Akeyazi terrane in Tianshan, China, interpreted from petrological and mineral zoning evidence, with *P–T* paths constrained from psuedosections (Li et al. 2016). García-Casco et al. (2002) modelled oscillatory zoning in garnet and amphibole chemistry from serpentinite mélange in Cuba, concluding that they formed in near equilibrium and record fluctuations in *P–T* conditions during subduction. Blanco-Quintero et al. (2011) also reported reburial during interpreted large-scale convective flow from this mélange, interpreted from garnet zoning and *P–T* pseudosection modelling. Geochronological constraints on the development of the mineral assemblages in the Port Macquarie eclogite point to a long history of high-pressure metamorphism, with a significant age difference between the formation of stage 1 and stage 2 assemblages (Fig. 15). Based on time scales of material movement in subduction systems from numerical modelling (Gerya et al. 2002), the geochronological data from the eclogite support the likelihood that multiple burial and partial exhumation paths may have occurred.

Subduction channel dynamics

A corner or return flow model of material within the subduction channel (e.g. Shreve and Cloos 1986, Gerya et al. 2002; Agard et al. 2009; Roda et al. 2019), is suggested for repeated burial and exhumation of the lawsonite eclogite at Port Macquarie. Numerical modelling predicts that during oceanic subduction, hydration of the mantle wedge creates a buoyant low viscosity serpentinite-filled subduction channel which can pluck high-pressure rocks from the subducting slab and circulate them within the channel (e.g. Gerya et al. 2002). In these models, the high-pressure fragments can become deeply subducted, but can also experience partial exhumation and reburial, resulting in *P–T* loops (Gerya et al. 2002). Rocks with different *P–T–t* histories can also accumulate within the channel and be exhumed together to form mélanges that contain a variety of subducted products (e.g. Krebs et al. 2008). At Port Macquarie, this behaviour is confirmed by the presence of garnet blueschist, which is ca. 470 Ma in age, and has a different *P–T* path to the eclogite, yet is found as a tectonic block less than 10 m away from the lawsonite eclogite (Och et al. 2003; Tamblyn et al. 2019a).

The geochronological data presented above also supports the notion of long-lived residence of high-pressure materials within oceanic subduction channels. The minimum duration spent in the subduction channel by the lawsonite eclogite at Port Macquarie is ca. 50 M y (Fig. 15). Analogous durations of high-pressure metamorphism and accumulation have been reported from oceanic subduction systems. Exotic high-pressure rocks hosted in serpentinite, which have been interpreted to have been buried and exhumed by convective flow processes, span an age range of ca. 55 M y. in Cuba (Lázaro et al. 2009), and ca. 40 M y. in the Dominican Republic (Krebs et al. 2008). High-pressure rocks exhumed in Turkey with different *P–T–t* histories span an age range of ca. 20 M y. (Pourteau et al. 2019), supported by in situ Ar–Ar data (Fornash et al. 2016). In the Mariana subdution system, the residence time for blueschist within the subduction channel is ca. 48 M y (Tamblyn et al. 2019b).

With the caveat that the *P–T* conditions suggested from the phase equilibrium modelling of the eclogite at Port Macquarie are taken as approximations, a *P–T–t* path can

be constructed for the lawsonite eclogite, and the rate of exhumation to reburial estimated. If the maximum possible *P–T* conditions of stage 1 exhumation are taken as 2.0 GPa and 500 °C, the total pressure and temperature change from peak stage 1 to peak stage 2 equates to ~ 1.6 GPa and 190 °C. If an average lithostatic pressure of 3.2 km/kbar with no non-lithostatic loads is assumed, this pressure change is equivalent to approximately 50 km of vertical depth change. Depending on subduction angle, the total travel distance of the lawsonite eclogite within the channel may have been more than 100 km during the looping *P–T* history.

Conclusions

Lawsonite eclogite in serpentinite melange at Port Macquarie in the Southern New England Orogen records *P–T* conditions of ~ 2.9 GPa and 600 °C, attained at ca. 500–490 Ma. The mineral assemblages that define these *P–T* conditions were overprinted by a second high-pressure assemblage that formed at ca. 450 Ma. Compositional zoning in phengite, and growth of a second generation of garnet, indicate the overprinting mineral assemblage formed during up-pressure metamorphism to ~ 2.7 GPa and 590 °C. Between these two stages of burial, partial exhumation occurred to at least 2.0 GPa, but probably to lower *P–T* conditions. The *P–T* evolution defines hairpin looping *P–T* paths that developed along a similar geothermal gradient, suggesting the lawsonite eclogite was cycled within a serpentinite-filled subduction channel during return flow of subducted material. This cycling occurred over a minimum timeframe of ca 50 M y., implying long-lived residence of the eclogite within the subduction system. A number of studies are beginning to discover that subducted material may undergo complex *P–T–t* evolutions that record multiple episodes of burial and exhumation during prolonged residence within subduction systems. These cyclic *P–T* evolutions support predictions from numerical models which suggest material can follow convective flow paths within evolving serpentinite-filled subduction channels.

Acknowledgements The authors would like to thank Ben Wade and Sarah Gilbert of Adelaide Microscopy, for their assistance with EPMA and LA–ICP–MS data collection. David Kelsey is thanked for helpful discussions and his ongoing support with phase equilibria modelling. Jack Gillespie of Curtin University is thanked for collecting the phase and EDS maps. Mitchell Bockmann of the University of Adelaide is thanked for setting up the titanite U–Pb method. We thank Pierre Lanari and an anonymous reviewer for their comments, which greatly strengthened the manuscript. This research in part was supported by Australian Research Council Grant DP160104637. Renée Tamblyn acknowledges support from the University of Adelaide in the form of the Aldermann Kleeman travel scholarship and an Australian Postgraduate Award.

Funding This research in part was supported by an Australian Research Council Grant (DP160104637). The contribution of Jack Gillespie was supported by an Australian Research Council Discovery Project (DP190103849). Part of this research was undertaken using SEM instrumentation (ARC LE190100176, LE140100150) at the John de Laeter Center, Curtin University. Renée Tamblyn acknowledges support from the University of Adelaide in the form of the Aldermann Kleeman travel scholarship and an Australian Postgraduate Award.

Availability of data and material All data presented in this manuscript can be found in the supplementary materials.

Compliance with ethical standards

Conflict of interest The authors declare no conflicts of interest or competing interests.

References

Agard P, Yamato P, Jolivet L, Burov E (2009) Exhumation of oceanic blueschists and eclogites in subduction zones: timing and mechanisms. Earth Sci Rev 92(1):53–79

Agard P, Plunder A, Angiboust S, Bonnet G, Ruh J (2018) The subduction plate interface: rock record and mechanical coupling (from long to short time scales). Lithos 320:537–566

Aitchison JC, Blake MC, Flood PG, Jayko AS (1994) Paleozoic ophiolitic assemblages within the southern New England orogen of eastern Australia: Implications for growth of the Gondwana margin. Tectonics 13(5):1135–1149. https://doi.org/10.1029/93TC03550

Anczkiewicz R, Burg J, Villa IM, Meier M (2000) Late Cretaceous blueschist metamorphism in the Indus suture zone, Shangla region, Pakistan Himalaya. Tectonophysics 324(1–2):111–134

Angiboust S, Agard P, Raimbourg H, Yamato P, Huet B (2011) Subduction interface processes recorded by eclogite-facies shear zones (Monviso, W. Alps). Lithos 127(1–2):222–238

Angiboust S, Pettke T, De Hoog JC, Caron B, Oncken O (2014) Channelized fluid flow and eclogite-facies metasomatism along the subduction shear zone. J Petrol 55(5):883–916

Blanco-Quintero IF, García-Casco A, Gerya TV (2011) Tectonic blocks in serpentinite mélange (eastern Cuba) reveal large-scale convective flow of the subduction channel. Geology 39(1):79–82

Bosse V, Féraud G, Ballevre M, Peucat J-J, Corsini M (2005) Rb–Sr and 40Ar/39Ar ages in blueschists from the Ile de Groix (Armorican Massif, France): implications for closure mechanisms in isotopic systems. Chem Geol 220(1–2):21–45

Bröcker M, Baldwin S, Arkudas R (2013) The geological significance of 40Ar/39Ar and Rb–Sr white mica ages from S yros and S ifnos, G reece: a record of continuous (re) crystallization during exhumation? J Metamorph Geol 31(6):629–646

Carswell D, Wilson R, Zhai M-G (2000) Metamorphic evolution, mineral chemistry and thermobarometry of schists and orthogneisses hosting ultra-high pressure eclogites in the Dabieshan of central China. Lithos 52(1–4):121–155

Castelli D, Rubatto D (2002) Stability of Al-and F-rich titanite in metacarbonate: petrologic and isotopic constraints from a polymetamorphic eclogitic marble of the internal Sesia Zone (Western Alps). Contrib Miner Petrol 142(6):627–639

Chakhmouradian AR (2004) Crystal chemistry and paragenesis of compositionally unique (Al-, Fe-, Nb-, and Zr-rich) titanite from Afrikanda. Russia Am Mineral 89(11–12):1752–1762

Collins WJ (2002) Nature of extensional accretionary orogens. Tectonics 21(4):6

Collins W, Richards S (2008) Geodynamic significance of S-type granites in circum-Pacific orogens. Geology 36(7):559–562
de Meyer CM, Baumgartner LP, Beard BL, Johnson CM (2014) Rb–Sr ages from phengite inclusions in garnets from high pressure rocks of the Swiss Western Alps. Earth Planet Sci Lett 395:205–216
Della Ventura G, Bellatreccia F, Williams C (1999) Zr-and LREE-rich titanite from Tre Croci, Vico volcanic complex (Latium, Italy). Mineral Mag 63(1):123–130
Di Vincenzo G, Tonarini S, Lombardo B, Castelli D, Ottolini L (2006) Comparison of 40Ar–39Ar and Rb–Sr data on phengites from the UHP Brossasco-Isasca Unit (Dora Maira Massif, Italy): implications for dating white mica. J Petrol 47(7):1439–1465
Diener J, Powell R (2012) Revised activity–composition models for clinopyroxene and amphibole. J Metamorph Geol 30(2):131–142
Elburg M, Bons P, Foden J, Brugger J (2003) A newly defined Late Ordovician magmatic-thermal event in the Mt Painter Province, northern Flinders Ranges, South Australia. Aust J Earth Sci 50(4):611–631
Elburg M, Vroon P, van der Wagt B, Tchalikian A (2005) Sr and Pb isotopic composition of five USGS glasses (BHVO-2G, BIR-1G, BCR-2G, TB-1G, NKT-1G). Chem Geol 223(4):196–207
Evans T (2004) A method for calculating effective bulk composition modification due to crystal fractionation in garnet-bearing schist: implications for isopleth thermobarometry. J Metamorph Geol 22(6):547–557
Fornash KF, Cosca MA, Whitney DL (2016) Tracking the timing of subduction and exhumation using 40 Ar/39 Ar phengite ages in blueschist-and eclogite-facies rocks (Sivrihisar, Turkey). Contrib Miner Petrol 171(7):67
Forster MA, Lister GS (2014) 40Ar/39Ar geochronology and the diffusion of 39Ar in phengite–muscovite intergrowths during step-heating experiments in vacuo. Geol Soc Lond Spec Publ 378(1):117–135
Fukui S, Watanabe T, Itaya T, Leitch EC (1995) Middle Ordovician high PT metamorphic rocks in eastern Australia: evidence from K–Ar ages. Tectonics 14(4):1014–1020
Gaidies F, De Capitani C, Abart R (2008) THERIA_G: a software program to numerically model prograde garnet growth. Contrib Miner Petrol 155(5):657–671
García-Casco A, Torres-Roldán R, Millán G, Monié P, Schneider J (2002) Oscillatory zoning in eclogitic garnet and amphibole, Northern Serpentinite Melange, Cuba: a record of tectonic instability during subduction? J Metamorph Geol 20(6):581–598
Gerya TV, Stöckhert B, Perchuk AL (2002) Exhumation of high-pressure metamorphic rocks in a subduction channel: a numerical simulation. Tectonics 21(6):6
Glen R (2013) Refining accretionary orogen models for the Tasmanides of eastern Australia. Aust J Earth Sci 60(3):315–370
Glodny J, Bingen B, Austrheim H, Molina JF, Rusin A (2002) Precise eclogitization ages deduced from Rb/Sr mineral systematics: the Maksyutov complex, Southern Urals. Russia Geochim Cosmochim Acta 66(7):1221–1235
Green E, Holland T, Powell R (2007) An order-disorder model for omphacitic pyroxenes in the system jadeite-diopsidehedenbergite-acmite, with applications to eclogitic rocks. Am Miner 92(7):1181–1189
Hartnady MI, Kirkland CL, Clark C, Spaggiari CV, Smithies RH, Evans NJ, McDonald BJ (2019) Titanite dates crystallization: slow Pb diffusion during super-solidus re-equilibration. J Metamorph Geol 37(6):823–838
Hayden LA, Watson EB, Wark DA (2008) A thermobarometer for sphene (titanite). Contrib Miner Petrol 155(4):529–540
Hetzel R, Romer RL (2000) A moderate exhumation rate for the high-pressure Maksyutov Complex, southern Urals. Russia Geol J 35(3–4):327–344
Hogmalm KJ, Zack T, Karlsson AK-O, Sjöqvist AS, Garbe-Schönberg D (2017) In situ Rb–Sr and K-Ca dating by LA-ICP-MS/MS: an evaluation of N 2 O and SF 6 as reaction gases. J Anal At Spectrom 32(2):305–313
Holland T, Powell R (1998) An internally consistent thermodynamic data set for phases of petrological interest. J Metamorph Geol 16(3):309–343
Holland T, Powell R (2003) Activity–composition relations for phases in petrological calculations: an asymmetric multicomponent formulation. Contrib Miner Petrol 145(4):492–501
Holland T, Powell R (2011) An improved and extended internally consistent thermodynamic dataset for phases of petrological interest, involving a new equation of state for solids. J Metamorph Geol 29(3):333–383
Hyppolito T, Cambeses A, Angiboust S, Raimondo T, García-Casco A, Juliani C (2019) Rehydration of eclogites and garnet−replacement processes during exhumation in the amphibolite facies. Geol Soc London Spec Publ 478(1):217–239
Itaya T, Tsujimori T (2015) White mica K-Ar geochronology of Sanbagawa eclogites from Southwest Japan: implications for deformation-controlled K–Ar closure temperature. Int Geol Rev 57(5–8):1014–1022
Jenkins R, Landenberger B, Collins W (2002) Late Palaeozoic retreating and advancing subduction boundary in the New England fold belt, New South Wales. Aust J Earth Sci 49(3):467–489
Jessop K, Daczko N, Piazolo S (2019) Tectonic cycles of the New England Orogen, eastern Australia: a review. Aust J Earth Sci 66(4):459–496
Kabir M, Takasu A (2010) Evidence for multiple burial–partial exhumation cycles from the Onodani eclogites in the Sambagawa metamorphic belt, central Shikoku. Jpn J Metamorph Geol 28(8):873–893
Kelley S (2002) Excess argon in K–Ar and Ar–Ar geochronology. Chem Geol 188(1):1–22
Kemp A, Hawkesworth C, Collins W, Gray C, Blevin P (2009) Isotopic evidence for rapid continental growth in an extensional accretionary orogen: The Tasmanides, eastern Australia. Earth Planet Sci Lett 284(3):455–466
Kohn MJ (2004) Oscillatory-and sector-zoned garnets record cyclic (?) rapid thrusting in central Nepal. Geochem Geophys Geosyst 5(12).
Konrad-Schmolke M, O'Brien PJ, Zack T (2011) Fluid migration above a subducted slab—constraints on amount, pathways and major element mobility from partially overprinted eclogite-facies rocks (Sesia Zone, Western Alps). J Petrol 52(3):457–486
Krebs M, Maresch W, Schertl H-P, Münker C, Baumann A, Draper G, Idleman B, Trapp E (2008) The dynamics of intra-oceanic subduction zones: a direct comparison between fossil petrological evidence (Rio San Juan Complex, Dominican Republic) and numerical simulation. Lithos 103(1):106–137
Krebs M, Schertl H-P, Maresch W, Draper G (2011) Mass flow in serpentinite-hosted subduction channels: *P–T–t* path patterns of metamorphic blocks in the Rio San Juan mélange (Dominican Republic). J Asian Earth Sci 42(4):569–595
Lanari P, Engi M (2017) Local bulk composition effects on metamorphic mineral assemblages. Rev Mineral Geochem 83(1):55–102
Lázaro C, García-Casco A, Rojas Agramonte Y, Kröner A, Neubauer F, Iturralde-Vinent M (2009) Fifty-five-million-year history of oceanic subduction and exhumation at the northern edge of the Caribbean plate (Sierra del Convento mélange, Cuba). J Metamorph Geol 27(1):19–40
Leake BE, Woolley AR, Arps CE, Birch WD, Gilbert MC, Grice JD, Hawthorne FC, Kato A, Kisch HJ, Krivovichev VG (1997) Report. Nomenclature of amphiboles: report of the subcommittee on amphiboles of the international mineralogical association

commission on new minerals and mineral names. Mineral Mag 61(2):295–321
Leitch E (1975) Plate tectonic interpretation of the Paleozoic history of the New England Fold Belt. Geol Soc Am Bull 86(1):141–144
Li J-L, Klemd R, Gao J, John T (2016) Poly-cyclic metamorphic evolution of eclogite: evidence for multistage burial–exhumation cycling in a subduction channel. J Petrol 57(1):119–146
Liati A, Theye T, Fanning CM, Gebauer D, Rayner N (2016) Multiple subduction cycles in the Alpine orogeny, as recorded in single zircon crystals (Rhodope zone, Greece). Gondwana Res 29(1):199–207
Liferovich RP, Mitchell RH (2005) Composition and paragenesis of Na-, Nb- and Zr-bearing titanite from Khibina, Russia, and crystal-structure data for synthetic analogues. Can Mineral 43(2):795–812
Ludwig KR (2003) User's manual for IsoPlot 3.0. A geochronological toolkit for Microsoft Excel 71
Manton RJ, Buckman S, Nutman AP, Bennett VC, Belousova EA (2017) U-Pb-Hf-REE-Ti zircon and REE garnet geochemistry of the Cambrian Attunga eclogite, New England Orogen, Australia: implications for continental growth along eastern Gondwana. Tectonics 36(8):1580–1613
Marmo B, Clarke G, Powell R (2002) Fractionation of bulk rock composition due to porphyroblast growth: effects on eclogite facies mineral equilibria, Pam Peninsula, New Caledonia. J Metamorph Geol 20(1):151–165
Martin LA, Rubatto D, Brovarone AV, Hermann J (2011) Late Eocene lawsonite-eclogite facies metasomatism of a granulite sliver associated to ophiolites in Alpine Corsica. Lithos 125(1–2):620–640
Moresi L, Betts P, Miller M, Cayley R (2014) Dynamics of continental accretion. Nature 508(7495):245–248
Och DJ (2007) Eclogite, serpentinite, mélange and mafic intrusive rocks: manifestation of long-lived Palaeozoic convergent margin activity, Port Macquarie, eastern Australia.
Och D, Leitch E, Caprarelli G, Watanabe T (2003) Blueschist and eclogite in tectonic melange, port macquarie, New South Wales, Australia.
Och D, Zwingmann H, Philips G, Leitch E (2010) K–Ar dating of serpentinisation using fuchsite mica: the Rocky Beach metamorphic melange, Port Macquarie.
Park C, Song Y, Kang I-M, Shim J, Chung D, Park C-S (2017) Metasomatic changes during periodic fluid flux recorded in grandite garnet from the Weondong W-skarn deposit, South Korea. Chem Geol 451:135–153
Paton C, Hellstrom J, Paul B, Woodhead J, Hergt J (2011) Iolite: Freeware for the visualisation and processing of mass spectrometric data. J Anal At Spectrom 26(12):2508–2518
Phillips D, Harris J (2008) Provenance studies from 40 Ar/39 Ar dating of mineral inclusions in diamonds: methodological tests on the Orapa kimberlite, Botswana. Earth Planet Sci Lett 274(1):169–178
Phillips G, Offler R (2011) Contrasting modes of eclogite and blueschist exhumation in a retreating subduction system: The Tasmanides, Australia. Gondwana Res 19(3):800–811
Phillips G, Wilson CJ, Phillips D, Szczepanski SK (2007) Thermochronological (40Ar/39Ar) evidence of Early Palaeozoic basin inversion within the southern Prince Charles Mountains, East Antarctica: implications for East Gondwana. J Geol Soc 164(4):771–784
Phillips G, Landenberger B, Belousova E (2011) Building the New England Batholith, eastern Australia—Linking granite petrogenesis with geodynamic setting using Hf isotopes in zircon. Lithos 122(1–2):1–12
Phillips G, Offler R, Rubatto D, Phillips D (2015) High-pressure metamorphism in the southern New England Orogen: implications for long-lived accretionary orogenesis in eastern Australia. Tectonics 34(9):1979–2010
Pourteau A, Scherer EE, Schorn S, Bast R, Schmidt A, Ebert L (2019) Thermal evolution of an ancient subduction interface revealed by Lu–Hf garnet geochronology, Halilbağı Complex (Anatolia). Geosci Front 10(1):127–148
Powell R, Holland T (1988) An internally consistent dataset with uncertainties and correlations: 3. Applications to geobarometry, worked examples and a computer program. J Metamorph Geol 6(2):173–204
Putlitz B, Cosca M, Schumacher J (2005) Prograde mica 40Ar/39Ar growth ages recorded in high pressure rocks (Syros, Cyclades, Greece). Chem Geol 214(1–2):79–98
Roberts J, James L (2010) Stratigraphic relationships of Carboniferous volcanogenic successions in the Clifton-Carroll block and Werrie syncline, northern Tamworth Belt, southern New England Orogen. Aust J Earth Sci 57(2):193–205
Roda M, Zucali M, Regorda A, Spalla MI (2020) Formation and evolution of a subduction-related mélange: the example of the Rocca Canavese Thrust Sheets (Western Alps). GSA Bull 132(3–4):884–896
Rodrıguez J, Cosca M, Ibarguchi JG, Dallmeyer R (2003) Strain partitioning and preservation of 40Ar/39Ar ages during Variscan exhumation of a subducted crust (Malpica–Tui complex, NW Spain). Lithos 70(3–4):111–139
Rubatto D, Regis D, Hermann J, Boston K, Engi M, Beltrando M, McAlpine SR (2011) Yo-yo subduction recorded by accessory minerals in the Italian Western Alps. Nat Geosci 4(5):338
Sano S, Offler R, Hyodo H, Watanabe T (2004) Geochemistry and chronology of tectonic blocks in serpentinite mélange of the southern New England Fold Belt, NSW, Australia. Gondwana Res 7(3):817–831
Seifert W (2005) REE-, Zr-, and Th-rich titanite and associated accessory minerals from a kersantite in the Frankenwald, Germany. Mineral Petrol 84(3–4):129–146
Seifert W, Kramer W (2003) Accessory titanite: an important carrier of zirconium in lamprophyres. Lithos 71(1):81–98
Shaw S, Flood R (1981) The New England Batholith, eastern Australia: geochemical variations in time and space. J Geophys Res: Solid Earth 86(B11):10530–10544
Shreve RL, Cloos M (1986) Dynamics of sediment subduction, melange formation, and prism accretion. J Geophys Res: Solid Earth 91(B10):10229–10245
Spandler C, Hammerli J, Sha P, Hilbert-Wolf H, Hu Y, Roberts E, Schmitz M (2016) MKED1: a new titanite standard for in situ analysis of Sm–Nd isotopes and U–Pb geochronology. Chem Geol 425:110–126
Spear FS (1988) Metamorphic fractional crystallization and internal metasomatism by diffusional homogenization of zoned garnets. Contrib Miner Petrol 99(4):507–517
Spencer K, Hacker B, Kylander-Clark A, Andersen T, Cottle J, Stearns M, Poletti J, Seward G (2013) Campaign-style titanite U–Pb dating by laser-ablation ICP: Implications for crustal flow, phase transformations and titanite closure. Chem Geol 341:84–101
Stöckhert B, Gerya TV (2005) Pre-collisional high pressure metamorphism and nappe tectonics at active continental margins: a numerical simulation. Terra Nova 17(2):102–110
Tamblyn R, Hand M, Kelsey D, Anczkiewicz R, Och D (2019a) Subduction and accumulation of lawsonite eclogite and garnet blueschist in eastern Australia. J Metamorph Geol 38(2):157–182
Tamblyn R, Zack T, Schmitt A, Hand M, Kelsey D, Morrissey L, Pabst S, Savov I (2019b) Blueschist from the Mariana forearc records long-lived residence of material in the subduction channel. Earth Planet Sci Lett 519:171–181
Tsujimori T, Ernst W (2014) Lawsonite blueschists and lawsonite eclogites as proxies for palaeo-subduction zone processes: a review. J Metamorph Geol 32(5):437–454

Tsujimori T, Sisson VB, Liou JG, Harlow GE, Sorensen SS (2006) Very-low-temperature record of the subduction process: a review of worldwide lawsonite eclogites. Lithos 92(3):609–624

Vermeesch P (2018) IsoplotR: a free and open toolbox for geochronology. Geosci Front 9(5):1479–1493

Viete DR, Hacker BR, Allen MB, Seward GG, Tobin MJ, Kelley CS, Cinque G, Duckworth AR (2018) Metamorphic records of multiple seismic cycles during subduction. Sci Adv 4(3):0234

Vuorinen JH, Hålenius U (2005) Nb-, Zr-and LREE-rich titanite from the Alnö alkaline complex: crystal chemistry and its importance as a petrogenetic indicator. Lithos 83(1–2):128–142

Warren C, Sherlock S, Kelley S (2011) Interpreting high-pressure phengite 40Ar/39Ar laserprobe ages: an example from Saih Hatat, NE Oman. Contrib Miner Petrol 161(6):991–1009

Wei C, Clarke G (2011) Calculated phase equilibria for MORB compositions: a reappraisal of the metamorphic evolution of lawsonite eclogite. J Metamorph Geol 29(9):939–952

White R, Powell R, Holland T (2007) Progress relating to calculation of partial melting equilibria for metapelites. J Metamorph Geol 25(5):511–527

Woodhead JD, Hergt JM (2001) Strontium, neodymium and lead isotope analyses of NIST glass certified reference materials: SRM 610, 612, 614. Geostand Newslett 25(2–3):261–266

Zack T, Hogmalm KJ (2016) Laser ablation Rb/Sr dating by online chemical separation of Rb and Sr in an oxygen-filled reaction cell. Chem Geol 437:120–133